Synthesis of Novel Copper(I) Precursors for Atomic Layer Deposition

Atilla C. Varga

Bachelor of Science (Honours)

In

Chemistry Concentration in Nanotechnology

Carleton University

Ottawa, Ontario

The undersigned hereby recommends the Department of Chemistry acceptance of this thesis, submitted by Atilla C. Varga in partial fulfilment of the requirements for the degree of Bachelor of Science with Honors, Concentration in Nanotechnology.

Thesis Supervisor

TABLE OF CONTENTS

Table of Figures	3
Table of Equations	4
Table of Schemes	4
Abbreviations	5
Acknowledgements	6
Abstract	7
1 Introduction	8
1.1 Atomic Layer Deposition	8
1.1.1 ALD Growth Characteristics	9
1.2 Precursor Design	12
1.2.1 Volatility	13
1.2.2 Thermal Stability	16
1.2.3 Self-limiting Ligand Chemistry	17
2 Results and discussion	20
2.1 Copper(I) Precursor Synthesises	20
2.1.1 NHC Copper(I) Trifluoromethyl	
2.1.2 NHC Copper(I) Methyl(trimethylsilyI)	26
2.2 Thermogravimetric Analysis	
2.3 Differential Scanning Calorimetry	
2.4 Surface Saturation	
3 Conclusion	
4 Experimental	
4.1 General Methods	
4.2 Atomic Layer Deposition	
4.3 Synthetic Methods	
4.3.1 1,3-diisopropylimidazolidinium tetrafluoroborate (1)	
4.3.2 1,3-diisopropalimidazolium copper(I) chloride (2)	
4.3.3 [1,3-diisopropalimidazolium copper(I) tert-butoxide] ₂ (3)	
4.3.4 1,3-diisopropalimidazolium copper(I) trifluoromethyl (4)	
4.3.5 1,3-diisopropalimidazolium copper(I) methyl(trimethylsilyl) (5)	
5 References	
6 Appendicies	
Appendix A	
Appendix B	53

TABLE OF FIGURES

Figure 1. ALD layer by layer growth scheme9
Figure 2. ALD precursor surface saturation behaviour
Figure 3. ALD growth per cycle linear behaviour11
Figure 4. General structure of NHCs with unsaturated (imidazoline) and saturated
(imidazole) backbone on the left and right respectively
Figure 5. Stabilization of carbenic carbon lone pair achieved by electron donating due to
symmetry overlap of nitrogen orbitals with a vacant p-orbital on the carbon atom 18
Figure 6. Crystal structure of 2 . Thermal ellipsoids shown at 50% probability22
Figure 7. ¹⁹ F-NMR spectrum of the mixture of compounds obtained from the attempted
synthesis of 4
Figure 8. HSQC-NMR spectrum of ${\bf 5}$ shown the coupling between hydrogen labeled ${\bf H}_{\rm A}$
(on NeoSi ligand) across the copper atom to carbon labeled C_B (on NHC ligand) 28
Figure 9. TGA of 6.25 mg of compound 5 with blue trace being percent mass loss and
orange trace being derivative of percent mass with respect to temperature
Figure 10. Calculated partial pressure vs temperature relationship for 5 from Figure 9
TGA data and using Equation 2 31
Figure 11. DSC of 5 with onset of decomposition at 188 °C
Figure 12. Copper precursor figure of merit using Equation 3 , where red circles are
negative sigma values and blue are positive. Corresponding compounds labeled (from 1-
4, left to right) in figure and respective references (1&2 ¹⁴ , 3&4 ⁴⁰)34
Figure 13. QCM mass gain from ALD saturation experiment of compound 5 (0.264 g) with
a bubbler and line temperature of 150 °C and QCM temperature of 173 °C
Figure 14. Diagram of the ALD tool used equipped with a 6.985 cm inner diameter and
91.44 cm long stainless-steel furnace tube. With (a) being a steel cylindrical ball valve
bubbler, (b) is the carrier gas inlet and (c) is the secondary precursor inlet (which was
used for trimethyl aluminum) all equipped with ALD valves from Swagelok. (d) is a Baraton
capacitance manometer, (e) connects the system to a liquid nitrogen trap followed by a

roughing pump, (f) is the QCM component which extends into the center of t	he ALD
chamber and (g) is a mass spectrometer.	40
Figure 15. ¹ H NMR of compound 1 in CDCl ₃	50
Figure 16. ¹ H NMR of compound 2 in C ₆ D ₆	51
Figure 17. ¹ H NMR of compound 3 in C ₆ D ₆	51
Figure 18. ¹ H NMR of compound 4 in C ₆ D ₆	52
Figure 19. ¹ H NMR of compound 5 in C ₆ D ₆	52
TABLE OF EQUATIONS	
Equation 1. Sauerbrey equation for a QCM mass change from the change in res	sonance
frequency	12
Equation 2. Estimation of vapour pressure using TGA based on the Langmuir ed	•
Equation 3. Figure of merit calculation where T _D is the temperature of decompositi	
·	, ,
T _V is the vapour temperature at a specific pressure (°C), %m _{res} is the percent	
mass and %m _{Cu} is the percent mass of copper within the precursor	33
TABLE OF SCHEMES	
Scheme 1. Synthesis of 1 via the reaction of an orthoester with N,N'-diall	kyl-α,ω-
alkanediamine in the presence of ammonium tetrafluoroborate and done neat	20
Scheme 2. Deprotonation reaction of 1 using KOtBu in the presence of CuCl	to form
compound 2.	21
Scheme 3. Salt metathesis reaction of 2 and KO ^t Bu which initially forms a monor	mer that
is known to undergo a dimerization reaction to form 3	23
Scheme 4. Reaction of 3 with CF ₃ SiMe ₃ to form compound 4	24
Scheme 5. Grignard ligand exchange reaction of 2 and (trimethylsilyl)methyl mag	gnesium
chloride to synthesize 5	27

ABBREVIATIONS

ALD - Atomic Layer Deposition

DSC - Differential Scanning Calorimetry

GPC - Growth Per Cycle

MS – Mass Spectrometer

NHC - N-Heterocyclic Carbene

NMR - Nuclear Magnetic Resonance

QCM – Quartz Crystal Microbalance

SCCM – Standard Cubic Centimeter per Minute

SiG - Silicone Grease

TGA - Thermal Gravimetric Analysis

THF – Tetrahydrofuran

TMA – Trimethylaluminum

ACKNOWLEDGEMENTS

I would like to thank everyone who has helped me throughout the years and in accomplishing this thesis. From Dr. Seán Barry for letting me have this amazing opportunity and be apart of the Barry Lab. To all the great people in the Barry lab and especially Matthew Griffiths who has passed on so much of his great knowledge to me. And last but certainly not least my family, my awesome partner Ksenia who is always by my side and my parents who always are encouraging and willing help. Thank you all!

ABSTRACT

Copper metal thin films continue to be used as an interconnect material for silicon integrated circuits. Copper reduces propagation delays, power consumption, and size of the interconnects in the circuits, which makes it a highly sought-after metal in the field of nanotechnology. Atomic layer deposition (ALD) is a layer by layer, self-limiting, thin film deposition technique excels at depositing nanoscale films. However, the thickness of the copper film needs to be reduced to <2 nm to keep up with the ever-decreasing size. This implies that the ligand attached to the copper precursor needs to promote a self-limiting behaviour of the compound for better conformality and perform better than the currently available precursors. We can use N-heterocyclic carbenes (NHCs) as the self-limiting behaviour promoting ligand in ALD to increase the conformality of the film. Such a concept hasn't been described before in the field, although NHC's are known to bind strongly to metallic surfaces as a self-assembled monolayer. Our group has developed a general framework for coinage metal precursors where one ligand is the intended self-limiting ligand (NHC) and the other ligand leaves the surface upon chemisorption. The above framework seems to work; however, the precursor is not thermodynamically stable enough to survive the delivery temperature. Therefore, different leaving ligands (CF3 and methyl(trimethylsilyl)) and a different NHC (isopropyl side groups) were synthesized and tested. The best leaving ligand was determined to be methyl(trimethylsilyl), which when paired with the isopropyl NHC sufficiently increased the thermal stability and volatility of the resulting precursor. The onset of thermal decomposition and 1 Torr temperature was 188 °C and 143 °C respectively, giving a thermal range of 45 °C.

1 INTRODUCTION

1.1 Atomic Layer Deposition

Atomic layer deposition (ALD) is a layer by layer, thin film deposition technique which has a wide range of applications, most notably in creating semiconductors. ^{1,2} ALD has gained significant interest within the semiconductor field due to continued decrease of device size which requires atomic level control over the thickness of deposited thin films. To achieve a good uniformity on such a small scale, it is required to have very good conformality on high aspect ratio features.³ Other thin film deposition techniques are unable to achieve the same conformality as ALD, since ALD is the only deposition technique which uses self-limiting surface reactions. Self-limiting surface reactions occur when the compound (which is being deposited) will only react with the substrate and not itself to create a monolayer (single molecule thick layer) across the entire surface.⁴ This allows for conformal coverage of all the substrates surface features (trenches, peaks, etc.) and is not effected by line of sight like other thin film deposition techniques.⁵

The process for depositing a metallic thin film by ALD is to sequentially expose (pulse) the surface with a precursor to create a monolayer and then a co-reagent to alter the composition of the monolayer and to reactivate it for further growth. A schematic of this sequential process is shown in **Figure 1**, where the blue with orange spheres represent the precursor and the red spheres represent the co-reagent which reacts at the surface to alter the chemical composition of the precursor to enable further deposition.

Purge steps are used to clear the deposition area of any unreacted precursor or coreagents.

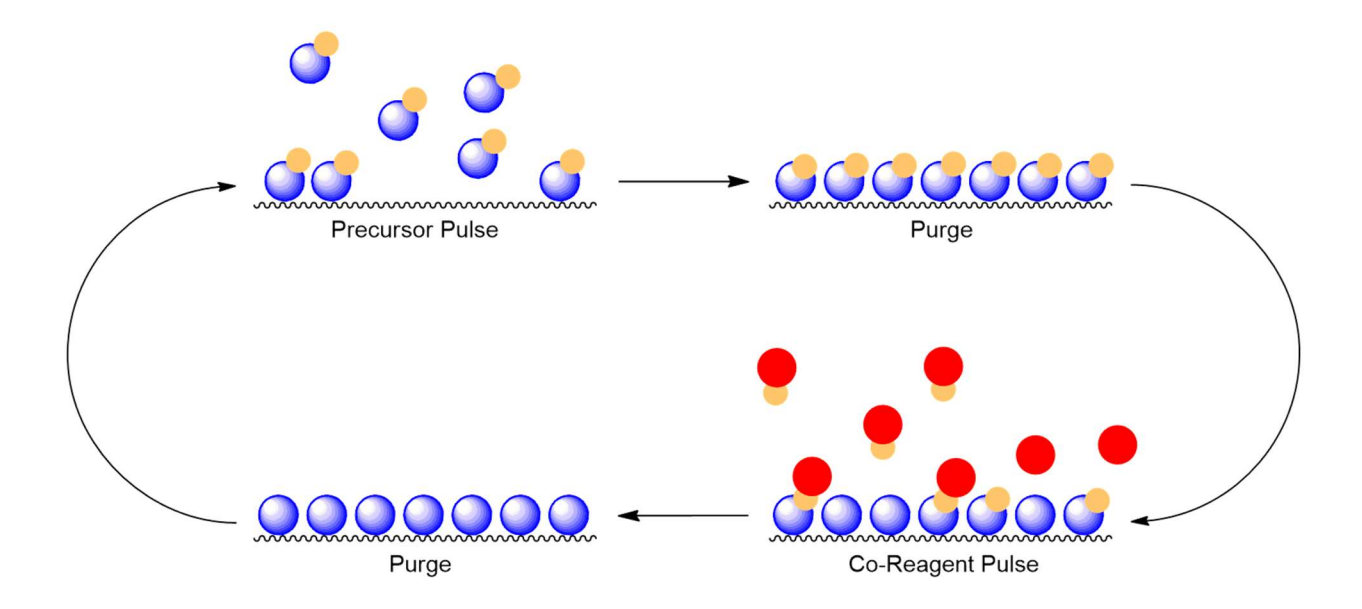


Figure 1. ALD layer by layer growth scheme.

The ALD sequential process from **Figure 1** can be repeated numerous times to create a film with the desired thickness. For ALD applications where an oxide or nitride thin film is required, the co-reagent is commonly the oxygen or nitrogen source. Then the sequential process is repeated in the same manner to create alternating metal-oxygen or metal-nitrogen layers which make up the thin film.⁶

1.1.1 ALD Growth Characteristics

ALD as previously noted is a self-limiting, saturative thin film deposition technique which means that during each precursor pulse the amount of precursor which reacts with the surface is determined and limited by a finite number of available surface binding sites.

The precursor should not react with itself once it has been chemisorbed to the surface

and once all surface sites are occupied, no further deposition will occur.⁷ This can be visualized by using a saturation curve (**Figure 2**) where the mass gain per ALD cycle is plotted against the pulse time of the precursor. Once all the surface sites are occupied the surface becomes saturated with precursor and the mass gain (film growth) stops.

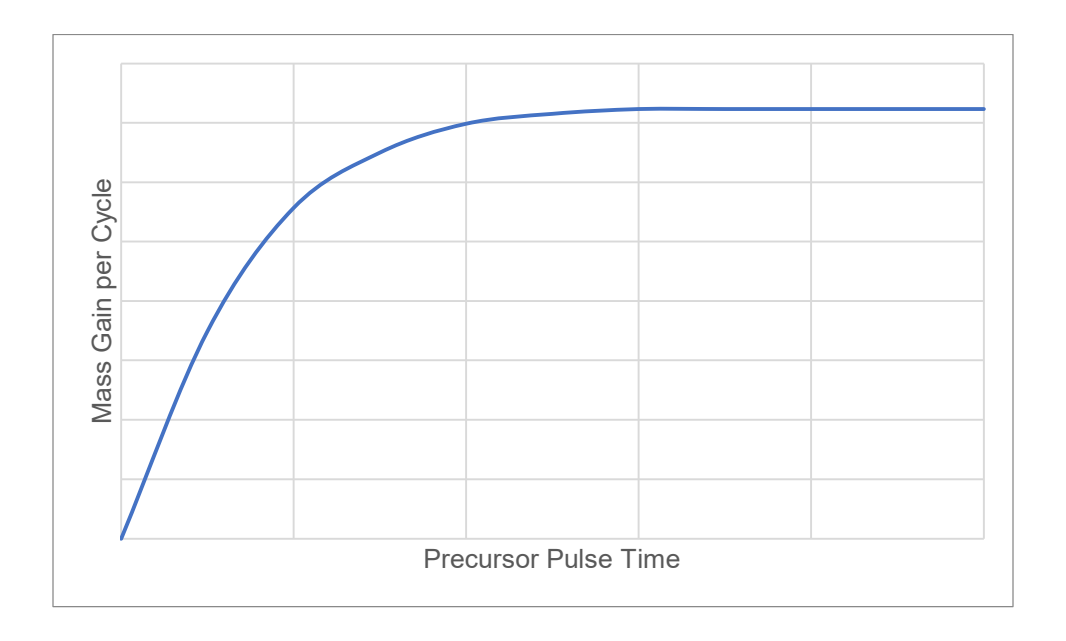


Figure 2. ALD precursor surface saturation behaviour.

The same phenomenon can be observed in a larger scope for the sequential, repeated ALD cycles. Since each precursor pulse will result in one additional monolayer (which has an associated thickness increase), the overall film thickness in relation to the number of cycles can be observed in **Figure 3**. The resulting linear relationship is very useful and desirable for thin film synthesis since atomic layer control (at an Angstrom level) can be achieved by altering the number of ALD cycles which directly corresponds to a known number of monolayers and intern thickness.⁸

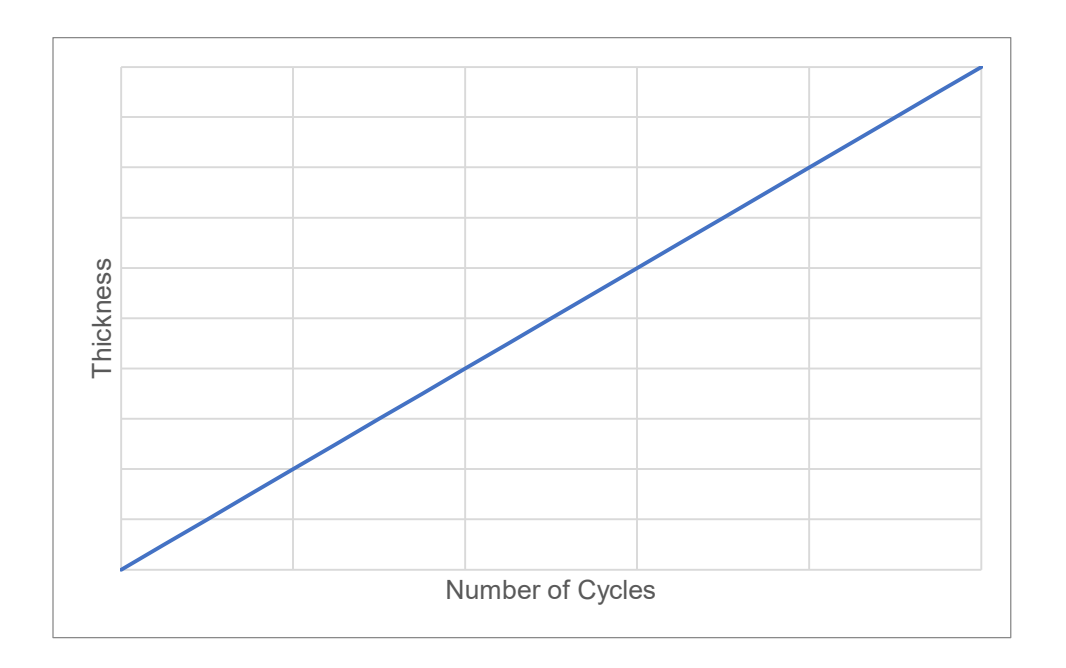


Figure 3. ALD growth per cycle linear behaviour.

Very selective, calculatable and predictable growth characteristics make ALD the ideal technique for creating nano scale, copper thin films used in microelectronics for the decreasing interconnects size.

To observe these growth characteristics, you need to be able to monitor the mass gain on the substrate surface *in-situ*, however these can be quite expensive and invasive to the deposition process.^{9,10} However, a straight-forward *in-situ* technique which is commonly used to measure the mass gain during ALD experiments is a quartz crystal microbalance (QCM). A QCM detects mass changes by measuring the change in frequency of a quartz crystal resonator. The resonant frequency of the quartz crystal changes when a small mass load is added to the crystal.¹¹ The change in resonant frequency can be used in the Sauerbrey equation to calculate the mass change.¹²

$$\Delta m = -C \frac{\Delta f}{n}$$

Equation 1. Sauerbrey equation for a QCM mass change from the change in resonance frequency

Where Δm is the mass change, C is the resonance frequency of the quartz crystal, Δf is the change in frequency and n is the odd overtone integer number (odd due to shearing vibration mode¹³).

1.2 Precursor Design

An ALD precursor is the chemical compound (reactant) which is used for delivering the desired element to the surface for deposition. The precursor will react with the surface by first physisorbing and then chemisorbing to create a surface-metal bond. There are different physical and chemical properties which determine the usefulness of a precursor discussed in this section.

ALD precursors come in a wide range of types: which heteroatoms are included (e.g., oxygen, nitrogen, silicon, etc.) and complexities (e.g., monomers, dimers, trimers, chelating). The commonality between all of them are a few key factors which need to be met: volatility and thermal stability. For common previously investigated copper precursors, the majority are oxygen containing and are based on older methodologies. ^{14–16} This is an issue since oxygen containing precursors can introduce oxygen impurities into the film which hinder the device performance. ¹⁷ In addition there has not been a organometallic (only Cu-C bonds) precursor created for copper; introducing such a

precursor would be a great addition to broadening the range of available copper precursors.

Another vital characteristic for ALD precursors is the self-limiting growth behaviour. A modern copper ALD process is needed to keep up with the modern-day decreasing size of microelectronic interconnects today. The need for self-limiting growth is increased with the smaller scale nanofabrication to maintain a reliable uniform film. Moreover, at such a scale there is little to no room for film imperfections. The goal of this thesis was to develop a new type of Cu precursor with a deliberately designed self-limiting ligand and leaving ligand combination.

1.2.1 Volatility

For ALD precursors it is necessary that the compound can enter the gas phase without undergoing a chemical change and can be delivered to the deposition chamber of the ALD tool. The precursor must also volatilize at a temperature which is within the ALD tools range. This is usually well below the lowest melting point of the tool's components: a common target is <100 °C.

Traditional volatile ALD copper ligands can be grouped into two main groups: halides and aliphatic (including more complex chelating ligands). These ligands are used because they decrease the compounds overall volatility since they have low crystalline intramolecular interactions. For example, halides are known to experience weak intermolecular interactions in the solid state due to their high electronegativity. This is because halides (especially fluorine) are very hard and non-polarizable atoms which are

less likely to experience intermolecular interactions (such as induced dipole, dipole-dipole or hydrogen bonding). In addition, these types of ligands can be made to have more mobility so that in the solid phase, the packing is less compact and ordered. Combining the low intramolecular interactions with higher mobility, induces a low liquid-to-gas transition point of the complex which leads to a lower volatilization point. Two volatile copper ligands will be investigated, which include one bulky halide and one bulk aliphatic.

When considering a volatile halide precursor, the reactivity and nature of the ligand must be investigated. During the co-reagent ALD subcycle, the halide ligand will be removed from the metal center. Therefore, if a direct metal-halide bonded ligand is used, then during the co-reagent step (if H⁺ or H₂ are used) liberation of HX molecules will occur. This will result in problems such as etching of the film, corrosion of the ALD tool, or a toxic side product which then needs to be handled. ^{19,20} Hence direct metal-halide bonds will be avoided and copper-alkyl halide ligands, such as the more electronegative fluoroalkyl ligand CF₃ or aliphatic alkyls will be used.

For a volatile bulky alkyl ligand there are numerous variations for ligand choices. However, the key factor which can help narrow down a potential ligand is bulk. If the ligand is a long aliphatic chain or has a simple structure, it has a low number of degrees of freedom. The resulting compound in the crystalline solid phase would experience better stabilization and greater intermolecular interactions.²¹ As mentioned above, less interactions result in better volatility hence a more bulky (higher degrees of freedom) ligand would be beneficial. For such a ligand a larger four coordinate atom (such as silicon) can be used as the center to create the same tetrahedral geometry ligand

however, it occupies a larger volume.²² In recent years, methyl-trimethylsilyl (NeoSilyl ligand) has shown itself to have great promise as a ligand choice for ALD processes.²³ Hence it will be used in this work.

A method for analyzing and determining the volatility of an ALD precursor is by using thermogravimetric analysis (TGA). We can calculate the compounds vapour pressure using the following equation.

$$P = \frac{dm}{dt} \sqrt{\frac{T}{M} \cdot \frac{2\pi R}{\alpha}}$$

Equation 2. Estimation of vapour pressure using TGA based on the Langmuir equation.

Here, P is the vapour pressure at temperature T, dm/dt is the rate of mass loss per unit surface area which is obtained from a TGA temperature ramp experiment, R is the gas constant, M is the molecular mass of the compound and α is the vaporization coefficient. He vaporization coefficient is assumed to be 1 in a vacuum, however for the specific TGA used this value was calculated experimentally. This was done by using benzoic and salicylic acid which each have known literature parameters for **Equation 2** and solving for α . As mentioned above the equation is an estimation since it is based on the assumptions made by the Langmuir equation. Those assumptions include: it is an ideal gas system, a homogenous surface, energetically equivalent sites, molecules that do not interact, and identical mechanisms of desorption (volatilization) for the standard and test sample.

1.2.2 Thermal Stability

While any ALD precursor must be volatile it must also be thermally stable, meaning that during volatilization the precursor must not undergo decomposition. The precursor must also be stable at temperatures past its volatilization point so it can survive delivery and deposition during the ALD process. The ligand that remains with the metal center upon chemisorption (the "self-limiting ligand") in an ALD complex needs a strong metal – ligand bond since it needs to withstand any side reactions during chemisorption to ensure a complete self-limiting monolayer growth. Hence it is usually less of a concern than the other ligands.

Both the CF₃ and NeoSi leaving group ligands are expected to add to the thermal stability of an overall complex since they have no β-hydrogen atoms and thus cut off a common decomposition pathway (β-hydrogen elimination) for metal complexes. As mentioned above, both ligands have low molecular weights which requires less energy for volatilization. Hence if less energy is required to induce a gas-phase transition, the likelihood for decomposition is decreased.²⁵ In addition, both the CF₃ and NeoSi ligands have been used in other ALD processes where a clean volatilization with no thermal decomposition was observed.^{26–29}

A method for determining the thermal stability is differential scanning calorimetry (DSC). DSC is a calorimetry technique (measurement of heat by analysing the heat exchange between a sample and a reference)³⁰ which is used to measure the heat flow difference between a sample and a reference. The heat flow difference will result in exothermal (heat released by the sample) and endothermal (heat adsorbed by the

sample) events which can be used to determine phase changes, and most importantly onsets of thermal decomposition of a sample which are usually exothermal in nature.³¹ Hence this method will be used to examine the decomposition points of a potential copper precursor.

1.2.3 Self-limiting Ligand Chemistry

One of the most important aspects of an ALD precursor is the self-limiting surface chemistry behaviour, hence it is very important in precursor design. The goal of a self-limiting ligand is to create a strong ligand-surface bond (which can be broken afterwards) and prevent additional precursor bonding. This will create a monolayer of precursor during a deposition cycle.³²

$$R-N$$
 N
 R
 R
 N
 R

Figure 4. General structure of NHCs with unsaturated (imidazoline) and saturated (imidazole) backbone on the left and right respectively.

For coinage metals a ligand which shows very good potential as a self-limiting ligand are N-heterocyclic carbenes (NHCs) (See **Figure 4**). So called normal NHCs are based on an imidazole or imidazoline ring where N-C-N carbon bears a lone pair. This carbon atom is called the carbenic carbon since it has a lone pair of electrons in an sp² hybridized orbital.³³ The lone pair on the carbon is stabilized by electron donating due to symmetry overlap of the nitrogen orbitals with a vacant p orbital on the carbon (as shown

in **Figure 5**). The lone pair on the carbenic carbon is very nucleophilic and will donate electron density to the metal center creating a very strong ligand-metal bond.³⁴

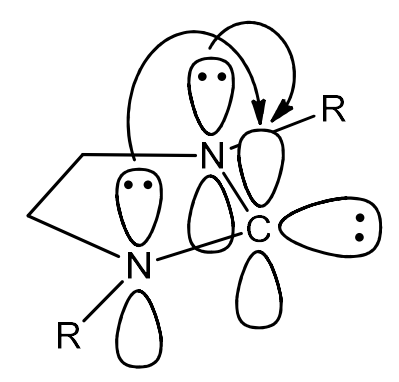


Figure 5. Stabilization of carbenic carbon lone pair achieved by electron donating due to symmetry overlap of nitrogen orbitals with a vacant p orbital on the carbon atom.

NHCs in other applications have been shown to create very strong self assembled monolayers (SAMs) on a gold surface.³⁵ Here, NHCs were used to displace very strong gold sulfide bonds, demonstrating the very strong bonding it has with coinage metals, and we expect it to be very promising for a self-limiting ligand when used in a copper precursor. A simple NHC with a small saturated backbone will be used as to help prevent any possible ligand decomposition.

In addition, the so called "wingtip" groups of the NHC (i.e., the N,N-substituents) play a key role in the ligand surface chemistry. If methyl groups are used, the NHC ligand binds to the metal surface by lying down flat instead of standing perpendicular in an η^1 fashion.³⁶ In the same work, isopropyl groups were used which enforced perpendicularly binding to copper or gold surface, allowing for closer packing. This closer and more dense

packing create a more uniform conformal SAM, showing great promise as an ALD precursor ligand.

In this thesis, two potential ALD precursors will be examined where both are structured around the same design. Both will have an intended leaving group ligand which (ideally) will leave once the precursor chemisorbs to the surface. One of such ligands will be a CF₃ and the other a NeoSi. The second ligand will be the self-limiting ligand which will remain bonded to the copper atom after chemisorption and inhibit addition precursor deposition. This ligand will be an unsaturated NHC with isopropyl side groups and will be the same for each precursor.

2 RESULTS AND DISCUSSION

2.1 Copper (I) Precursor Synthesises

For the copper(I) precursors which were synthesized and will be discussed, the following starting materials and reactions were performed.

$$\begin{array}{c|c} & & & \\ &$$

Scheme 1. Synthesis of **1** via the reaction of an orthoester with N,N'-dialkyl- α , ω -alkanediamine in the presence of ammonium tetrafluoroborate and done neat.

The one-pot synthesis of **1** was carried out in a straightforward neat reaction following a literature preparation as shown in **Scheme 1**.³⁷ After workup, an ¹H-NMR spectrum of the solid off-white needles was taken and the sample was not pure and needed to be further recrystalized. After the additional recrystallization, the solid needles became whiter, ¹H-NMR spectroscopy showed no signs of impurities (shown in **Figure 15**), and a ¹⁹F-NMR spectrum displayed two isotopic peaks at -153 ppm which is characteristic of fluorine coupling to two isotopes of boron (with spin numbers of 3/2 and 1/2) in a BF₄ salt. The compound was then used for further reactions.

Scheme 2. Deprotonation reaction of **1** using KO^tBu in the presence of CuCl to form compound **2**.

The synthesis of **2** (**Scheme 2**) involved the deprotonation of the carbene salt to form the free carbene which then ligates the acidic CuCl. Potassium tert-butoxide was used to deprotonate the carbene salt and produce insoluble by-products which were removed by filtration along with any excess copper chloride, during workup. An ¹H-NMR spectrum of the resulting solid white powder was recorded (shown in **Figure 16**) and the success of the reaction was determined by the lack of any fluorine peaks (which would indicate the presence of starting material) in a ¹⁹F-NMR spectrum.

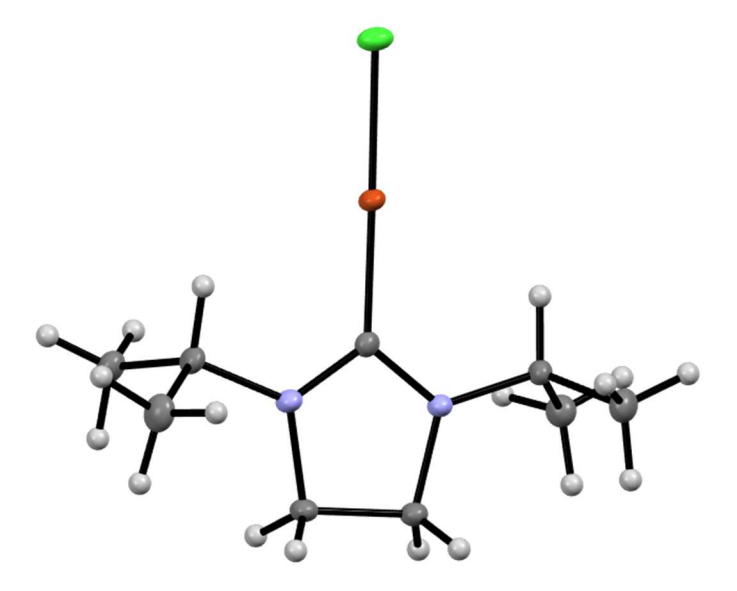


Figure 6. Crystal structure of 2. Thermal ellipsoids shown at 50% probability.

Crystals of compound **2** were also grown for crystallographic determination by dissolving the solid white powder in a minimal amount of a 2:1 (hexane to THF) solvent ratio and placed in a freezer at -24°C overnight. Finally, the excess solvent was decanted, and the sample was placed back in the freezer for an additional 24 hr.

2.1.1 NHC Copper (I) Trifluoromethyl

From the starting material **2**, the CF₃ precursor synthesis was performed by a modified preparation for active trifluoromethylating agents.³⁸

$$\begin{array}{c|c}
Cl \\
Cu \\
\hline
N
\end{array}$$

$$\begin{array}{c|c}
Cl \\
\hline
Cu \\
\hline
N
\end{array}$$

$$\begin{array}{c|c}
Cu \\
\hline
N
\end{array}$$

Scheme 3. Salt metathesis reaction of **2** and KO^tBu which initially forms a monomer that is known to undergo a dimerization reaction to form **3**.

Compound 2 was reacted with potassium tert-butoxide to undergo a salt metathesis reaction which forms an initial monomer and insoluble KCI. The monomer then undergoes a dimerization reaction to form 3, bridging through the tert-butoxide ligands. Compound 3 is reported to be thermally unstable and was filtered, then usually used immediately for subsequent reactions.

However, an attempt was made to isolate the intermediate product for characterization to ensure that the chemistry was working properly. This involved a filtration workup step to remove the insoluble KCI, followed by simply removing the solvent. An ¹H-NMR spectrum of **3** was recorded (shown in **Figure 17**) and it can be seen from the hydrogen integration ratios (which should be 12:9:4:2, with 9 being the tert-butoxide hydrogens) that the decomposition of the compound is quite extensive. After 20 minutes the integration ratios were 12:5:4:2 which show that the decomposition reduces the tert-butoxide hydrogen integration. This indicates that the compound is either losing bridging tert-butoxide ligands or the compound is no longer a dimer, rendering the immediate use of **3** very important.

Scheme 4. Reaction of **3** with CF₃SiMe₃ to form compound **4**.

The final reaction to synthesize the target CF₃ precursor involves the reaction of **3** with two equivalents of CF₃(SiMe₃) trimethylsilyl compound. The product of this reaction was a yellow oil, as expected from the literature preparation. After work up, needle-like yellow crystals were obtained. An ¹H-NMR spectrum of the compound was taken (shown in **Figure 18**) and the product had small amounts of THF impurities; triplets found at 3.57 and 1.42 ppm. Half the ¹H-NMR peaks were not consistent with the literature values however the integrations and splitting patters were all indicative of the product. An ¹⁹F-NMR spectrum of the compound was also taken and shown below.

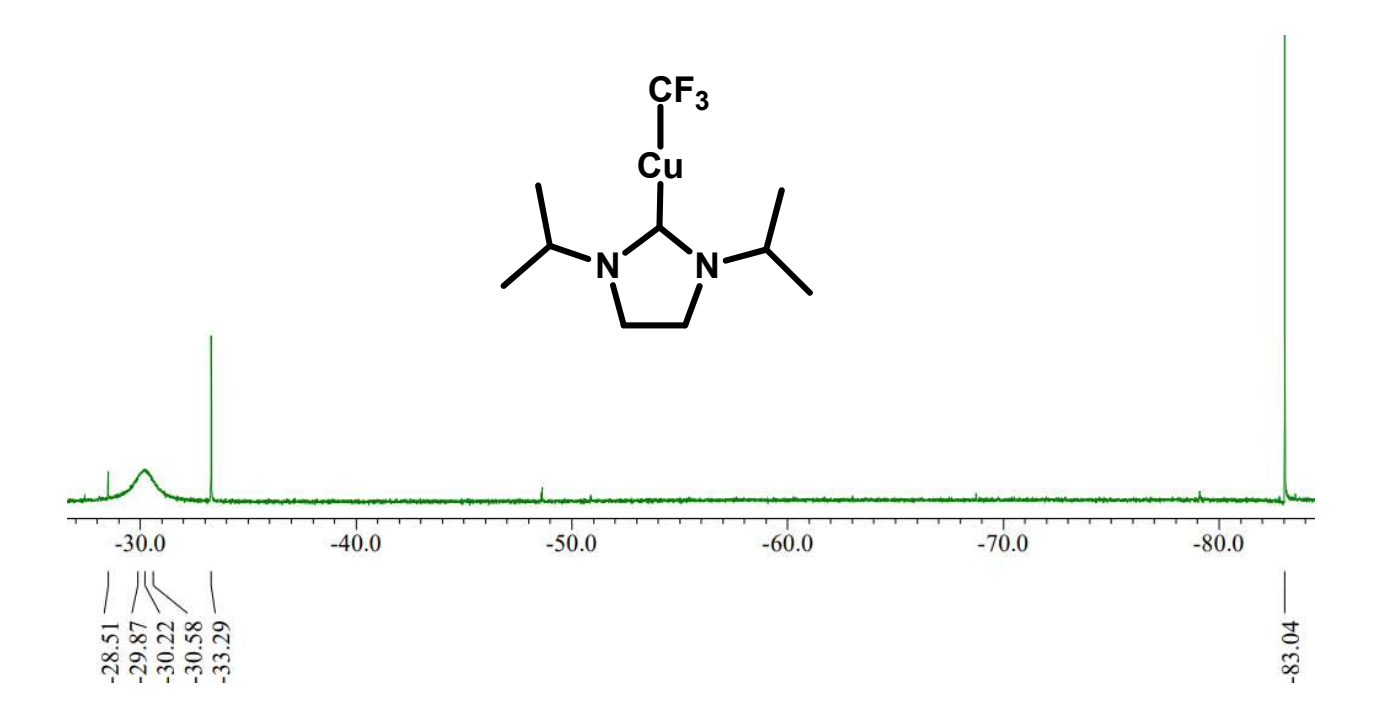


Figure 7. ¹⁹F-NMR spectrum of the mixture of compounds obtained from the attempted synthesis of **4**.

As seen from **Figure 7** there are four peaks in the ¹⁹F-NMR spectrum which for compound **4** would be expected to have only one. The three fluorine atoms in the compound all experience the same chemical environment and should only produce one peak. This peak would be expected to be present at -33 ppm.³⁸ There is a peak present at -33 ppm which indicates the correct compound and along with the ¹H-NMR spectrums (shown in **Figure 18**) peak splittings and integrations are all in accordance with the literature spectrum. However, there is a peak with a much greater intensity at -83 ppm and two other peaks (one sharp and one broad) at -28 and -30 ppm respectively. The ¹⁹F-NMR spectrum showed that more than one fluorine-containing species was present in the product. Hence further characterization was required.

A sample of crystals were used in crystallographic determination to gain further insight into the structure of the compound. The results were inconclusive, as there were multiple structures in the sample and differentiation between them was unsuccessful. However, some of the compound **2** starting material was isolated and a crystal structure was collected (shown in **Figure 6**). This could have affected the ¹H-NMR spectrum of **4** and could have been the source of the peak shifts. Since compounds **2** and **4** both have the same integrations and splitting patterns, the peak shifts would have been a combination of the two compounds. In addition, the possible contaminants found in the ¹⁹F-NMR spectrum would not have any ¹H-NMR spectrum peaks, dissolve in a polar solvent and be able to withstand a high vacuum. Some possibilities could include, chlorine containing species (such as CF₃CI), and/or silicon containing species (such as SiF₄ or SiF₃CI).

Many more attempts of different purification steps (different solvents and solvent ratio crystallizations, filtration, etc.) and re-attempted synthesizes were performed, but we were unable to isolate the product from this mixture of compounds. As such we were not able to determine the thermal properties of the desired Cu-CF₃ precursor.

2.1.2 NHC Copper (I) Methyl(trimethylsilyl)

The second targeted copper precursor was also synthesized using the same starting material **2** using the following synthetic strategy.

Scheme 5. Grignard ligand exchange reaction of **2** and (trimethylsilyl)methyl magnesium chloride to synthesize **5**.

Compound 2 was reacted with a Grignard reagent to exchange the methyl(trimethylsilyl) of the Grignard with the chloride of the NHC. This resulted in compound 5 and a magnesium (II) chloride precipitate which was filtered off during work up. In the first synthesis reaction, the product was an off-white powder which required purification by sublimation to remove any remaining starting material. However, in subsequent reactions 5 was recrystalized (initially to grow crystals) which resulted in a better yield and higher purity sample by ¹H-NMR spectroscopy (shown in **Figure 19**). The recrystallization was preformed using a 2:1 solvent ratio of Hexane to THF, which resulted in white bulky crystals.

Finally, both a HSQC- and HMBC-NMR spectrum were taken of **5** to ensure the successful addition of the NeoSi group onto the copper atom. Since the ¹H-NMR and ¹³C-NMR spectrum of the combined two salt starting materials would have identical spectrum as **5**, the addition NMR technique was required. The HMBC-NMR spectrum would show a hydrogen coupling from the NeoSi ligand across the copper to the carbenic carbon indicating compound **5** (shown below in **Figure 8**).

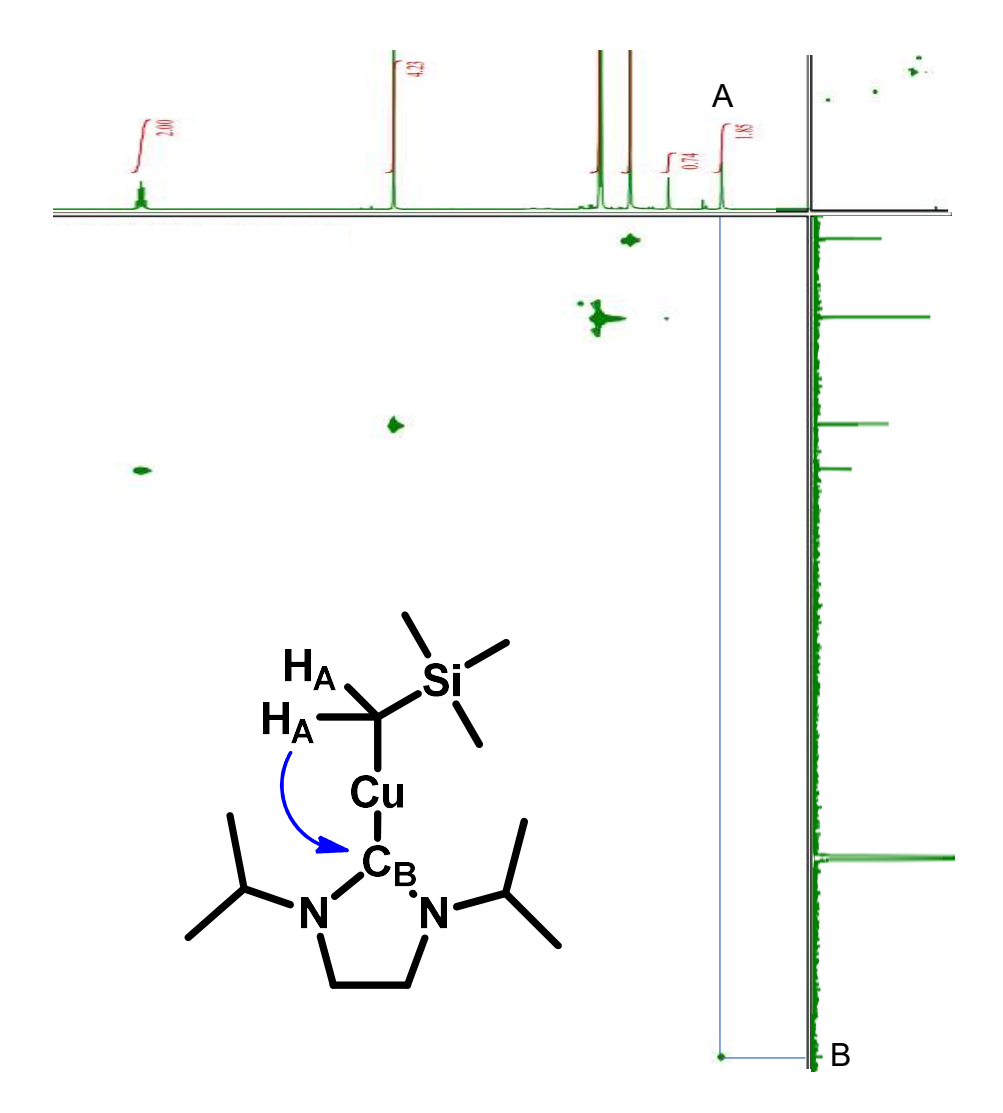


Figure 8. HSQC-NMR spectrum of **5** shown the coupling between hydrogen labeled H_A (on NeoSi ligand) across the copper atom to carbon labeled C_B (on NHC ligand).

As seen above by the blue line, this indicates that H_A couples to C_B across the copper atom (shown by the blue arrow). Hence the formation of **5** was successful since both the NeoSi and NHC ligands are attached to the copper atom and the 1H -NMR and 1G -NMR spectrums are not a combination of the two salts.

2.2 Thermogravimetric Analysis

Compound **5** was analyzed by TGA to determine its volatility and thermal stability. A simple temperature ramp experiment of 10 °C/min was performed with a sample mass of 6.25 mg.

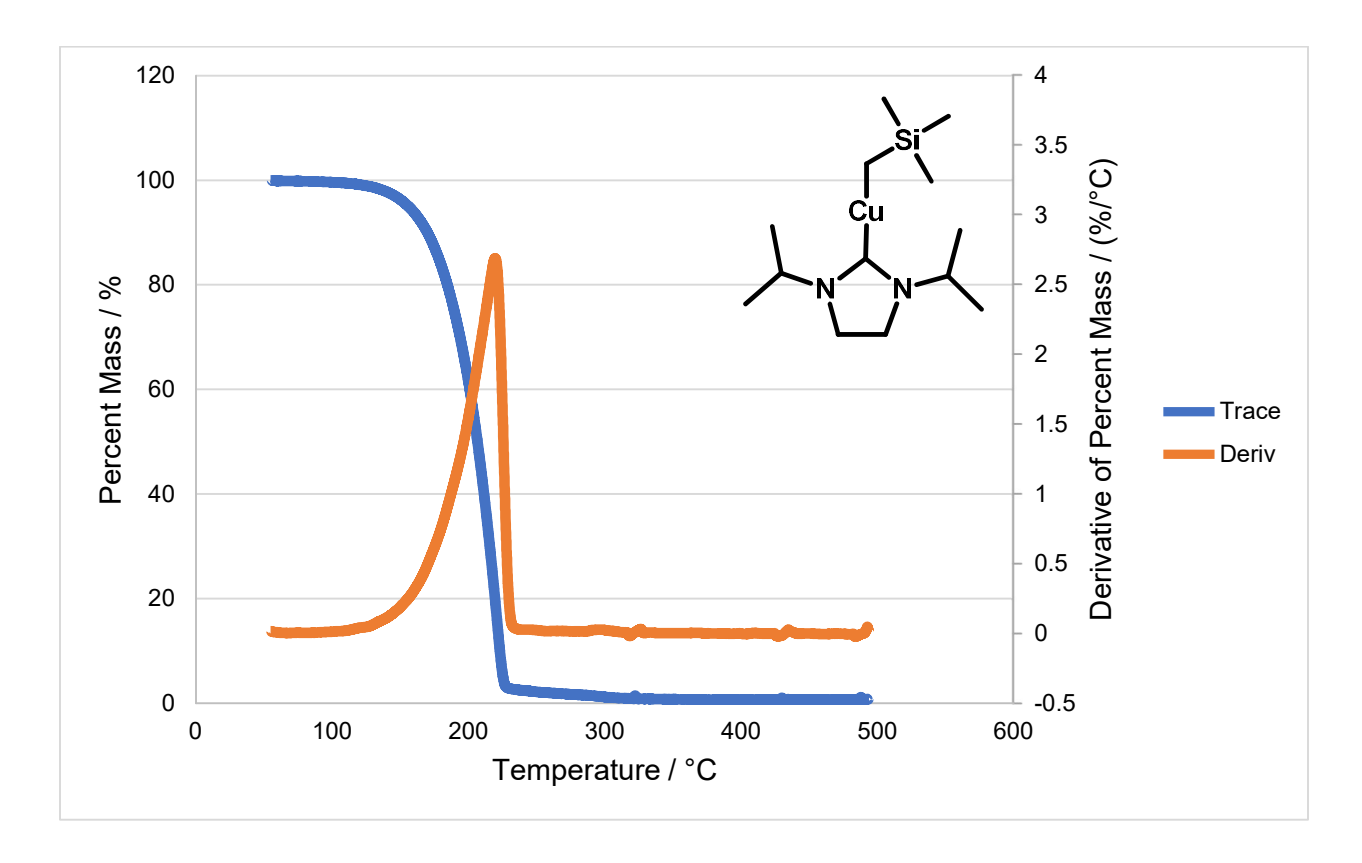


Figure 9. TGA of 6.25 mg of compound **5** with blue trace being percent mass loss and orange trace being derivative of percent mass with respect to temperature.

The onset of vaporization of a compound can be calculated from a TGA by the point at which the compound has lost 1% mass. At this point the compound begins to volatilize and can be used as a means of comparing volatility between compounds. For **5** the onset of vaporization is at 100 °C. The residual mass of a precursor is the percentage

of mass which did not volatilize by the end of the TGA experiment. This yields information of the thermal stability of the compound: if there is mass remaining after the temperature ramp experiment, then some amount of precursor decomposed and did not evaporate. For **5** there is a thermal change characteristic of volatilization, ending with ~5% residual mass. At around 230 °C the slope of the trace changes and the mass decreases more gradually indicating decomposition of the residual mass has occurred. This could be due to some of NeoSi ligand decomposing, since it has a weaker bonding to copper compared to the NHC. In the end of the TGA experiment, the residual mass is <0.5% which can be attributed to the slight decomposition which is seen after 230 °C and other impurities in the sample.

In addition, the derivative trace from the TGA experiment is a measure of the percent mass loss with respect to temperature. For a completely thermally stable and volatile compound this trace should follow an exponential increase followed by a sharp drop off to zero once all the compound has volatilized. Any deviations from this pattern or dramatic exponential slope changes would indicate a different rate of volatilization which means the precursor is decomposing and volatilizing at a different rate. Compound **5** has a very clean exponential volatilization rate and then a sharp drop off up to 230 °C where the slope changes slightly, showing that the sample is thermally stable up to around 230 °C from TGA experiments.

Furthermore, the TGA data can be used to calculate a compounds 1 Torr temperature. This is done by taking the derivative data and using **Equation 2**, to calculate the partial pressure of the compound at a given temperature. This data is then plotted

using the natural logarithm of evaporation rate vs. inverse temperature to get a linear relationship, as shown below.

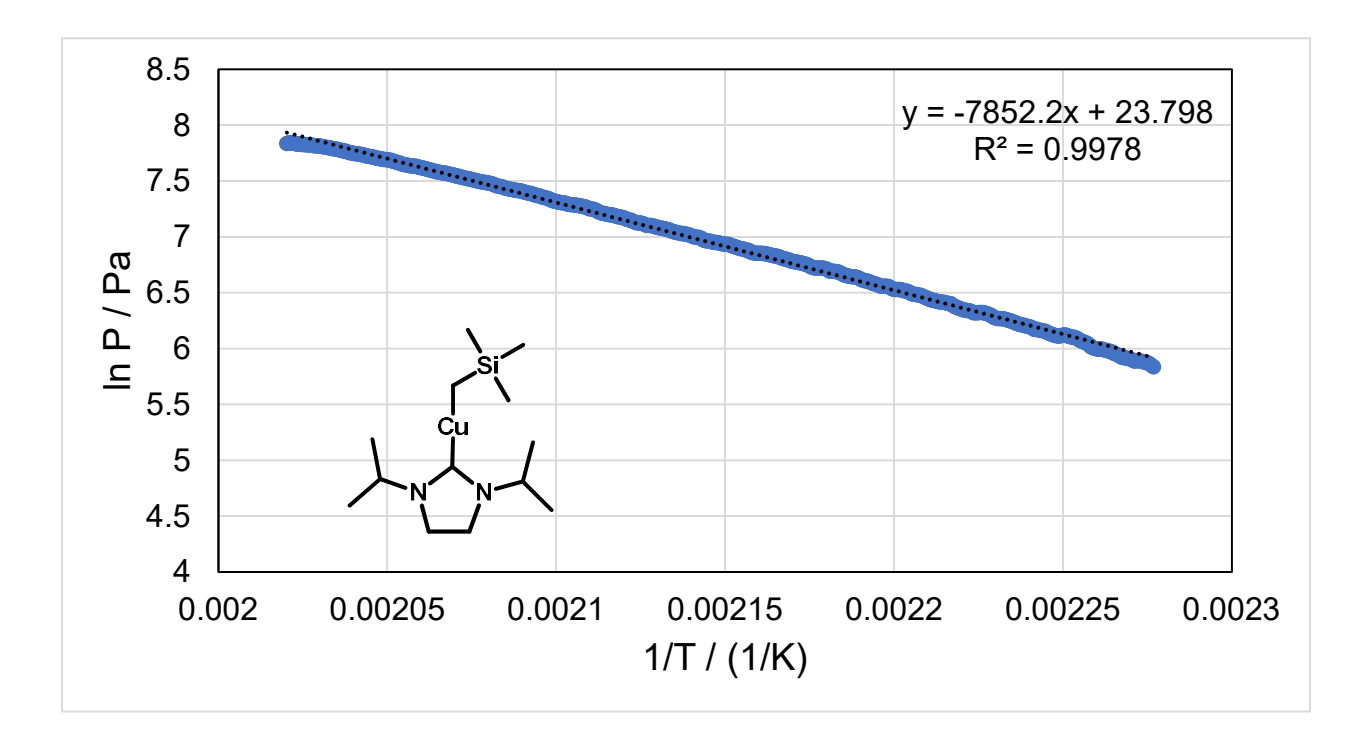


Figure 10. Calculated partial pressure vs temperature relationship for **5** from **Figure 9** TGA data and using **Equation 2**.

From the linear fit equation, the desired 1 Torr temperature can be determined calculated and for **5** the 1 Torr temperature is 143 °C with an error of ±0.3 °C. The 1 Torr temperature of an ALD precursor is very important regarding deposition. During an ALD experiment, there needs to be a significant amount of precursor in the gas phase to ensure that the growth surface can be saturated with precursor. This also means that when setting up an ALD experiment, the 1 Torr temperature will often be used as the bubbler and chamber temperature to ensure optimal precursor delivery.

2.3 Differential Scanning Calorimetry

The next step for precursor characterization was to investigate the thermal stability of the compound. This was done by analyzing **5** by DSC to determine any melting or decomposition points generally appear as exothermal (positive heat flow) and melting points or other phase transitions which appear as endothermal (negative heat flow when temperature is increased).

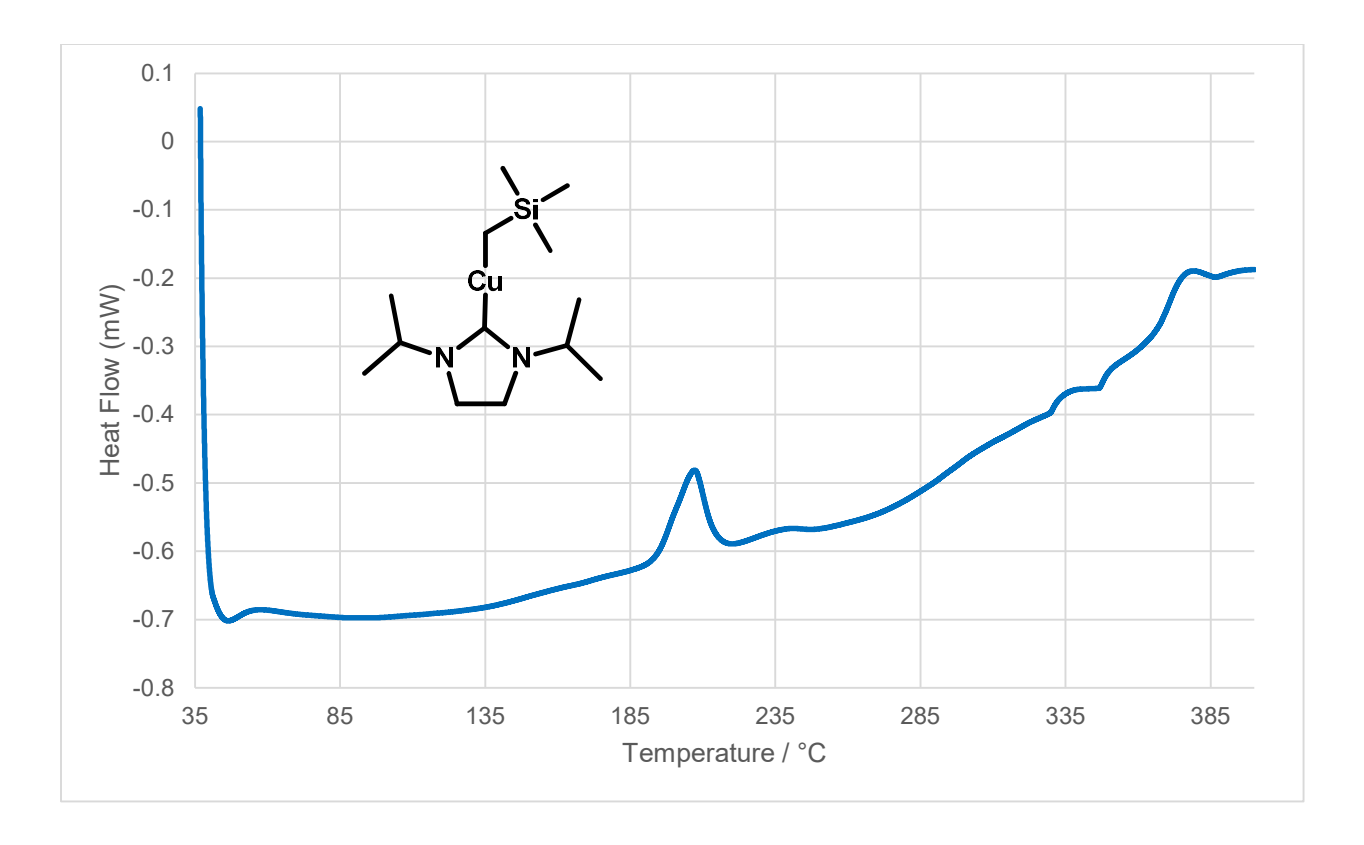


Figure 11. DSC of 5 with onset of decomposition at 188 °C

The above DSC analysis of compound **5** shows a very distinct exothermal peak with a maximum at 200 °C which corresponds to the decomposition of the compound.

Then there is an endothermal peak with a minimum at 46 °C which would correspond to the melting point of **5**.

The onset of this thermal decomposition is the value where the line tangent to the exothermal peak intersects the baseline. At this point the compound begins to decompose and is at 188 °C for **5**. This value was determined by the DSC analysis software.

From all this characterization data, a precursor figure of merit can be applied to the precursor as a visual representation for its usefulness.³⁹ This allows the precursor **5** to be compared to other copper precursors. The figure of merit is calculated based on the following equation.

$$\sigma = (T_D - T_V) \times \left(1 - \frac{\%m_{res}}{\%m_{Cu}}\right)$$

Equation 3. Figure of merit calculation where T_D is the temperature of decomposition (°C), T_V is the vapour temperature at a specific pressure (°C), %m_{res} is the percent residual mass and %m_{Cu} is the percent mass of copper within the precursor.

Using the calculated 1 Torr temperature (from TGA data), the residual mass (from TGA data), the onset of thermal decomposition (from DSC data) and the molecular weight of the compound can be plugged into **Equation 3** to calculate the figure of merit (σ). A positive value will represent a good ALD precursor where a negative value is representative of a less favourable precursor. Moreover, the larger the positive value the better the precursor. Sigma can then be plotted in a minefield chart against other copper precursors as a comparison (shown in **Figure 12** below).

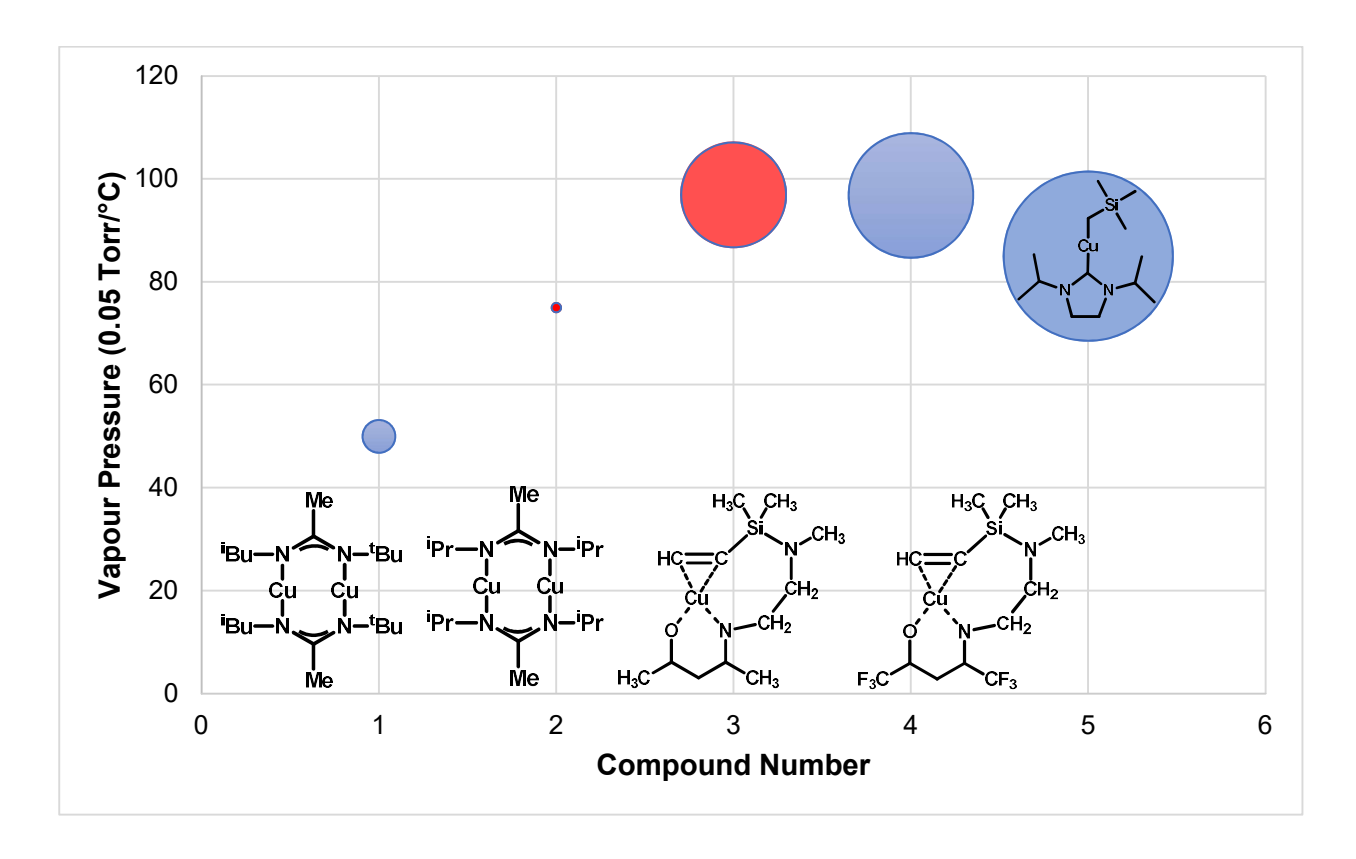


Figure 12. Copper precursor figure of merit using **Equation 3**, where red circles are negative sigma values and blue are positive. Corresponding compounds labeled (from 1-4, left to right) in figure and respective references (1&2¹⁴, 3&4⁴⁰).

As seen in **Figure 12**, compound **5** has the largest positive sigma value from the figure of merit calculation. This is due to the large difference between the 1 Torr temperature and the onset of thermal decomposition. Also compound **5** has a slightly lower residual mass than the other copper precursors showing that it would be preferential to the others.

2.4 Surface Saturation

From the TGA and DSC analysis of compound **5**, the onset of vaporization (100 °C), the 1 Torr temperature (143 °C) and onset of thermal decomposition (188 °C) meant that the precursor had very good properties for an ALD precursor. The precursor would begin to volatilize at a relatively low temperature, the precursor would have a large partial pressure under vacuum for deposition and the precursor would only begin to decompose well above its onset of vaporization. Resulting in a deposition temperature range of 88 °C with an ideal deposition range of 45 °C (from 1 Torr temperature up to decomposition point).

The final characteristic of the precursor which needed to be evaluated is its ability to undergo self-limiting chemisorption. This would be a proof-of-concept experiment to demonstrate the compounds ability to behave as an ALD precursor. This was evaluated by performing a surface saturation deposition experiment, where a large amount of precursor would be dosed into the deposition chamber for a long period of time. A QCM would be used *in-situ* to measure the mass gain from the precursor. If the precursor has a self-limiting characteristic, then there would be a rapid increase in growth on the QCM followed by a plateau where the surface would be saturated, and no more precursor would be able to react even though the precursor was still present about the QCM. The bubbler and deposition chamber were set at 150 and 175 °C respectively which is above the 1 Torr temperature and below the onset of thermal decomposition to ensure optimal growth and precursor dosage. Precursor pulse time was set to 6 minutes with an initial mass of

0.246 g and a nitrogen flow rate of 100 SCCM. The QCM was coated in aluminum oxide to emulate the growth on a silicon oxide surface for microelectronics fabrication.

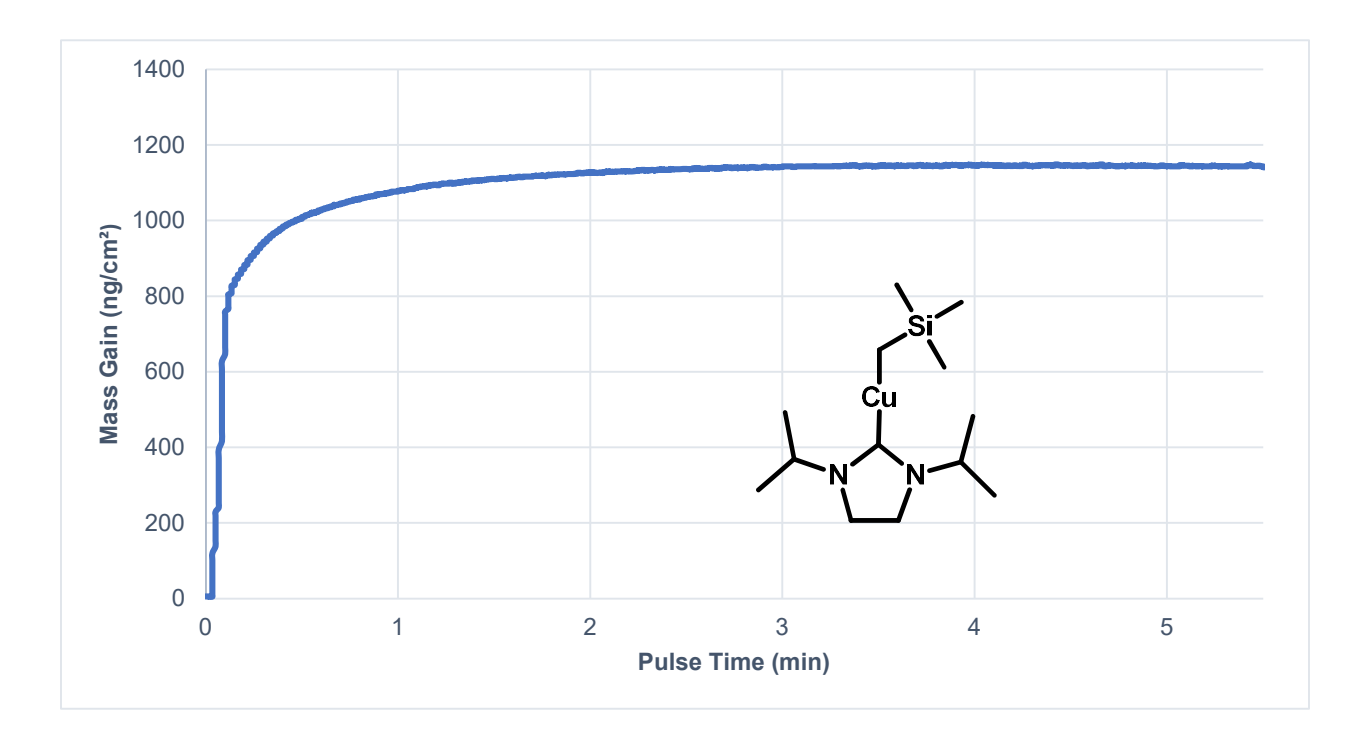


Figure 13. QCM mass gain from ALD saturation experiment of compound **5** (0.264 g) with a bubbler and line temperature of 150 °C and QCM temperature of 173 °C.

As seen above, the initial mass gain from the precursor is very large and exponential, however after 30 seconds the rate of mass gain begins to decrease. Then after 1 minute the mass gain plateaus off and for the following 5 minutes there is little to no additional mass recorded by the QCM. This is indicative of a good self-limiting ALD precursor growth. After the experiment was completed, there was 0.167 g of precursor left in the bubbler, meaning that the plateau of mass gain was not due to a lack of precursor but due to a self-limiting growth. In addition, there was a total of just under 1200 ng/cm³ of precursor deposited on the QCM's surface. The radius of the QCM is 0.7 cm, computing

a QCM surface area of 1.54 cm². Assuming a monolayer growth, the rough amount of precursor which was deposited onto the QCM surface was 1850 ng which is well below the spent precursor amount of 0.097 g.

Finally, the remaining precursor had a darkened charred color which indicates signs of decomposition, however once broken apart the inside revealed a lighter color on the interior. Unfortunately, an ¹H-NMR spectrum was not able to be run on the spent precursor due to university COVID-19 closures.

3 CONCLUSION

In conclusion, two copper ALD precursors where synthesized, one of which according to a literature preparation and one being novel. Both compounds (4 and 5) were synthesized from a common starting material 2 which was itself synthesized in 75% yield. Compounds 4 and 5 were synthesized in 56% and 87% cumulative yield respectively. All compounds 1-5 were characterized by ¹H-NMR spectroscopy, additionally compound 5 was characterized by ¹³C-NMR spectroscopy, 4 was characterized by ¹⁹F-NMR spectroscopy and 2 was characterized by crystallography.

TGA and DSC experiments were performed on **5** only, as **4** was unable to be successfully isolated. The resulting onset of vaporization, 1 Torr temperature and residual mass from TGA experiments for **5** was 100 °C, 143 °C and <0.5%. Then the onset of thermal decomposition from DSC experiments for **5** was 188 °C. This resulted in a useful deposition temperature range of 88 °C.

A surface saturation ALD experiment for **5** was completed at an optimal deposition temperature of 173 °C and bubbler plus lines temperature of 150 °C. Then 0.264 g of **5** was pulsed for 6 minutes over a QCM recording mass gain. Surface saturation was achieved after 1.5 minutes of pulse time with a final mass of 0.167 g of precursor. With slight charring of the final precursor, the above experiments render compound **5** to be a viable copper ALD precursor.

4 EXPERIMENTAL

4.1 General Methods

All reactions were carried out using oven-dried glassware in either a dry box or using Schlenk line techniques. Drybox syntheses were carried out in a MBraun Unilab inert atmosphere drybox, and solvents were purified through an MBraun solvent purification system. Unless otherwise noted, all reagents were purchased from commercially available sources and used as received (Millipore Sigma and Strem Chemicals). NMR spectra were recorded on a Bruker UltraShield 300 MHz or a JEOL 400 MHz spectrometer by dissolving 10 mg (for ¹H-NMR) and 100 mg (for ¹³C-NMR) in 0.75 mL of CDCl₃ or C₆D₆ as the solvent. Chemical shifts are reported in ppm with the residual solvent resonance as the internal standard. TGA experiments were performed TA Instruments Q50 apparatus installed in an MBraun Labmaster 130 Drybox under inert nitrogen atmosphere. Platinum pans were used as the holder and counterbalance for compound mass loading and temperature ramp experiments. The data which was recorded during the experiments was analyzed using TA Universal Analysis software. DSC experiments were performed on a TA Instruments Q10 apparatus with Q Series Pressure Cells as the compound holder and reference. The data which was recorded during the experiments was also analyzed using TA Universal Analysis software. Crystallography was preformed using the methods described in Appendix B.

4.2 Atomic Layer Deposition

ALD experiments were carried out in a hot-walled ALD reactor under inert atmospheric conditions, shown in **Figure 14** below:



Figure 14. Diagram of the ALD tool used equipped with a 6.985 cm inner diameter and 91.44 cm long stainless-steel furnace tube. With (a) being a steel cylindrical ball valve bubbler, (b) is the carrier gas inlet and (c) is the secondary precursor inlet (which was used for trimethyl aluminum) all equipped with ALD valves from Swagelok. (d) is a Baraton capacitance manometer, (e) connects the system to a liquid nitrogen trap followed by a roughing pump, (f) is the QCM component which extends into the center of the ALD chamber and (g) is a mass spectrometer.

A TAN06RCGP 6 MHz (14 mm) Polished Gold RC Quartz Crystal QCM from Colnatec was used for all mass gain data collection. The QCM was coated in aluminum

oxide using 100 cycles of trimethylaluminum (TMA) and water process.⁴¹ The ALD chamber was heated to 173 °C and the QCM was allowed to equilibrate overnight. The bubbler and all ALD lines were heated to 150 °C with a carrier gas (nitrogen >99.9999%) flow rate of 100 SCCM.

4.3 Synthetic Methods

4.3.1 1,3-diisopropylimidazolidinium tetrafluoroborate (1)

Triethyl orthoformate (1.482 g, 0.010 mol, 1.0 equiv), ammonium tetrafluoroborate (1.063 g, 0.010 mol, 1.0 equiv) and N,N-diisopropylethylenediamine (1.501 g, 0.010 mol, 1.0 equiv) were added to a 200 mL flask and heated at 120 °C in an oil bath for 3 hr. After cooling at room temperature, the ethanol formed during the reaction was evaporated on a rotary evaporator and the resulting white solid was further dried under high vacuum for 5 hr. This solid was crystallized from absolute ethanol to give white needles of the final product.³⁷

Yield: 2.0920 g (87 %). ¹H-NMR (400 MHz, CDCl₃): δ 8.09 (s, 0.99 H), 3.96 (q, 1.64 H), 3.93 (s, 4.00 H), 1.33 (d, 1.03 H). ¹³C-NMR (75 MHz, CDCl₃): δ 154.9, 50.7, 44.9, 20.6. ¹⁹F (376 MHz, CDCl₃): δ -153.0.

4.3.2 1,3-diisopropalimidazolium copper(I) chloride (2)

Compound **1** (4.022 g, 0.017 mol, 1.0 equiv) and copper (I) chloride (1.801 g, 0.018 mol, 1.1 equiv) were dissolved in 30 mL of THF in a 500 mL round bottom flask to which potassium tert-butoxide (1.861 g, 0.017 mol, 1.0 equiv) was added slowly. The solution turned dark grey upon addition and was stirred for 24 hr at room temperature. Solution

was then filtered through a pad of Celite and washed 2x times with 7 mL of THF. Filtrate was evaporated under high vacuum for 2 hr. The off-white residue was washed with pentane and filtered (product remained in frit). The product was recrystallized from a saturated 1:1 mixture of THF: pentane at -24 °C over 12 hr.

Yield: 3.096 g (75 %). 1 H-NMR (300 MHz, $C_{6}D_{6}$): δ 4.06 (sept, 2.00 H), 2.44 (s, 4.01 H), 0.70 (d, 12.17 H).

4.3.3 [1,3-diisopropalimidazolium copper(I) tert-butoxide]₂ (3)

Compound **2** (1.003 g, 0.004 mol, 2.0 equiv) was dissolved in 15 mL of THF in a 100 mL round bottom flask to which potassium tert-butoxide (0.455 g, 0.004 mol, 2.0 equiv) was added slowly. The solution was stirred for 2 hr at room temperature. This solution was then filtered through a pad of Celite and washed 2x times with 7 mL of THF. The product is not thermally stable at room temperature; therefore, filtrate was evaporated under high vacuum for 10 min. The white residue was washed with pentane and filtered (remained in frit) and used right away for subsequent reactions.

Yield: 0.410 g (69 %). ¹H-NMR (300 MHz, CDCl₃): δ 4.64 (m, 4.00 H), 2.73 (s, 3.87 H), 1.73 (s, 4.46 H), 0.94 (d, 11.98 H).

4.3.4 1,3-diisopropalimidazolium copper(I) trifluoromethyl (4)

Compound **3** (0.410 g, 0.002 mol, 1.0 equiv) was dissolved in 15 mL of THF in a 100 mL round bottom flask to which trifluoromethyltrimethylsilane (2.10 mL, 0.004 mol, 2.0 equiv, 2 M in THF) was added dropwise. The solution was stirred for 20 hr at room temperature. The solution was evaporated under high vacuum for 1 hr. Pale yellow oily

residue was washed with 2x times with 5 mL of pentane to remove impurities. The oily product was crystalized at -24 °C over 24 hr.

Yield: 0.374 g (86%). ¹H-NMR (300 MHz, C₆D₆): δ 4.06 (sept, 2.00 H), 2.54 (s, 4.19 H), 0.74 (d, 12.72 H). ¹⁹F (376 MHz, C₆D₆): δ -83.04 (s), -33.29 (s), -30.22 (b).

4.3.5 1,3-diisopropalimidazolium copper(I) methyl(trimethylsilyl) (5)

Compound **2** (0.224 g, 0.0009 mol, 1.0 equiv) was dissolved in 15 mL of THF in a 200 mL round bottom flask and cooled in a dry ice and acetone bath at -78 °C. (Trimethylsilyl)methyl magnesium chloride (2.262 mL, 0.001 mol, 1.0M, 1.1 equiv) was added dropwise over 5 minutes. The solution was stirred for 2 hr at -78 °C. The solution was then allowed to warm to room temperature and evaporated under high vacuum. The off-white solid was washed 2x times with 5 mL of pentane and filtered through a pad of Celite. The filtrate was evaporated under high vacuum for 2 hr and product was sublimed to result in a white solid. Alternatively, the product can be purified by recrystallization from a saturated 1:1 mixture of THF: pentane at -24 °C over 12 hr.

Yield: 0.248 g (87 %). ¹H-NMR (300 MHz, C₆D₆): δ 4.45 (sept, 2.00 H), 2.46 (s, 4.16 H), 0.83 (d, 12.63 H), 0.59 (s, 8.73 H), -0.12 (s, 1.94 H). ¹³C-NMR (75 MHz, C₆D₆): δ 201.7, 50.6, 41.8, 20.6, 5.0, -3.3.

5 REFERENCES

- Gordon, P. G.; Kurek, A.; Barry, S. T. JSS Focus Issue. Trends in Copper Precursor Development for CVD and ALD Applications. *ECS J. Solid State Sci. Technol.* 2015, 4 (1), 3188–3197. https://doi.org/10.1149/2.0261501jss.
- (2) George, S. M. Atomic Layer Deposition: An Overview. **1996**. https://doi.org/10.1021/cr900056b.
- (3) Puurunen, R. L. Surface Chemistry of Atomic Layer Deposition: A Case Study for the Trimethylaluminum/ Water Process. J. Appl. Phys 2005, 97, 121301. https://doi.org/10.1063/1.1940727.
- (4) George, S. M.; Ott, A. W.; Klaus, J. W. Surface Chemistry for ALD Growth; 1996.
- (5) Groner, M. D.; Elam, J. W.; Fabreguette, F. H.; George, S. M. *Electrical Characterization of Thin Al O Films Grown by Atomic Layer 2 3 Deposition on Silicon and Various Metal Substrates*; 2002; Vol. 413.
- (6) Fabreguette, F. H.; Wind, R. A.; George, S. M. Ultrahigh X-Ray Reflectivity from Multilayers Fabricated Using Atomic Layer Deposition. *Appl. Phys. Lett.* 2006, 88, 13116. https://doi.org/10.1063/1.2161117.
- (7) Dendooven, J.; Detavernier, C. Basics of Atomic Layer Deposition: Growth Characteristics and Conformality; 2017.
- (8) Hausmann, D. M.; Gordon, R. G. Surface Morphology and Crystallinity Control in the Atomic Layer Deposition (ALD) of Hafnium and Zirconium Oxide Thin Films. In

- Journal of Crystal Growth; 2003; Vol. 249, pp 251–261. https://doi.org/10.1016/S0022-0248(02)02133-4.
- (9) Alliata, D.; Kötz, R.; Novák, P.; Siegenthaler, H. Electrochemical SPM Investigation of the Solid Electrolyte Interphase Film Formed on HOPG Electrodes. *Electrochem. commun.* 2000, 2 (6), 436–440. https://doi.org/10.1016/S1388-2481(00)00056-4.
- (10) Wiesendanger, R. Scanning Probe Microscopy and Spectroscopy: Methods and Applications. Characterization of Solid Materials and Heterogeneous Cambridge University Press: Cambridge 1994, pp 57–60. https://doi.org/10.1017/CBO9780511524356.
- (11) King, W. H. Piezoelectric Sorption Detector. *Anal. Chem.* **1964**, *36* (9), 1735–1739. https://doi.org/10.1021/ac60215a012.
- (12) Sauerbrey, G. Verwendung von Schwingquarzen Zur W~igung Diinner Schichten Und Zur Mikrow~igung*; 1959; Vol. 55.
- (13) Cassiède, M.; Paillol, J. H.; Pauly, J.; Daridon, J. L. Electrical Behaviour of AT-Cut Quartz Crystal Resonators as a Function of Overtone Number. *Sensors Actuators, A Phys.* **2010**, *159* (2), 174–183. https://doi.org/10.1016/j.sna.2010.03.028.
- (14) Li, Z.; Barry, S. T.; Gordon, R. G. Synthesis and Characterization of Copper(I) Amidinates as Precursors for Atomic Layer Deposition (ALD) of Copper Metal. 2005. https://doi.org/10.1021/ic048492u.
- (15) Solanki, R.; Pathangey, B. ALD of Copper Seed Layers; 2000; Vol. 3.

- (16) Alnes, M. E.; Monakhov, E.; Fjellvåg, H.; Nilsen, O. Atomic Layer Deposition of Copper Oxide Using Copper(II) Acetylacetonate and Ozone. *Chem. Vap. Depos.* 2012, 18 (4–6), 173–178. https://doi.org/10.1002/cvde.201106959.
- (17) Becker, R.; Devi, A.; Weiß, J.; Weckenmann, U.; Winter, M.; Kiener, C.; Becker, H.-W.; Fischer, R. A. A Study on the Metal Organic CVD of Pure Copper Films from Low Cost Copper(II) Dialkylamino-2-Propoxides: Tuning the Thermal Properties of the Precursor by Small Variations of the Ligand. *Chem. Vap. Depos.* 2003, 9 (3), 149–156. https://doi.org/10.1002/cvde.200306236.
- (18) Devi, A. "Old Chemistries" for New Applications: Perspectives for Development of Precursors for MOCVD and ALD Applications. *Coordination Chemistry Reviews*. December 2013, pp 3332–3384. https://doi.org/10.1016/j.ccr.2013.07.025.
- (19) Putkonen, M.; Niinistö, L. Organometallic Precursors for Atomic Layer Deposition.2005, 9, 125–145. https://doi.org/10.1007/b136145.
- (20) Alexeeff, G. V.; Lewis, D. C.; Ragle, N. L. Estimation of Potential Health Effects from Acute Exposure to Hydrogen Fluoride Using a "Benchmark Dose" Approach. *Risk Anal.* 1993, 13 (1), 63–69. https://doi.org/10.1111/j.1539-6924.1993.tb00729.x.
- (21) Kim, T. K.; Lee, K. J.; Choi, M.; Park, N.; Moon, D.; Moon, H. R. Cite This. New J. Chem 2013, 37, 4130. https://doi.org/10.1039/c3nj00812f.
- (22) Zybill, C. The Coordination Chemistry of Low Valent Silicon; Springer, Berlin, Heidelberg, 1992; pp 1–45. https://doi.org/10.1007/3-540-54324-4_1.

- (23) Hatanpää, T.; Ritala, M.; Leskelä, M. Precursors as Enablers of ALD Technology: Contributions from University of Helsinki. *Coordination Chemistry Reviews*. December 2013, pp 3297–3322. https://doi.org/10.1016/j.ccr.2013.07.002.
- (24) Kunte, G. V.; Shivashankar, S. A.; Umarji, A. M. Thermogravimetric Evaluation of the Suitability of Precursors for MOCVD. *Meas. Sci. Technol.* 2008, 19 (2). https://doi.org/10.1088/0957-0233/19/2/025704.
- (25) Leskelä, M.; Ritala, M. Atomic Layer Deposition Chemistry: Recent Developments and Future Challenges. *Angewandte Chemie International Edition*. John Wiley & Sons, Ltd November 24, 2003, pp 5548–5554. https://doi.org/10.1002/anie.200301652.
- (26) Aaltonen, T.; Ritala, M.; Tung, Y.-L.; Chi, Y.; Arstila, K.; Meinander, K.; Leskelä, M. Atomic Layer Deposition of Noble Metals: Exploration of the Low Limit of the Deposition Temperature. **2020**. https://doi.org/10.1557/JMR.2004.0426.
- (27) Han, J. H.; Chung, Y. J.; Park, B. K.; Kim, S. K.; Kim, H.-S.; Kim, C. G.; Chung, T. *Chem. Mater* **2014**, *26*, 58. https://doi.org/10.1021/cm503112v.
- (28) Nam, W. H.; Rhee, S. W. Atomic Layer Deposition of ZrO2 Thin Films Using Dichlorobis[Bis-(Trimethylsilyl)Amido]Zirconium and Water. *Chem. Vap. Depos.* **2004**, *10* (4), 201–205. https://doi.org/10.1002/cvde.200306277.
- (29) Vehkamäki, M.; Hatanpää, T.; Kemell, M.; Ritala, M.; Leskelä, M. Atomic Layer Deposition of Ferroelectric Bismuth Titanate Bi₄Ti₃O₁₂ Thin Films. **2006**. https://doi.org/10.1021/cm060966v.

- (30) Ferrannini, E. The Theoretical Bases of Indirect Calorimetry: A Review.
 Metabolism. W.B. Saunders March 1, 1988, pp 287–301.
 https://doi.org/10.1016/0026-0495(88)90110-2.
- (31) Differential Scanning Calorimetry Günther Höhne, Wolfgang F. Hemminger, H.-J. Flammersheim.
- (32) Leskelä, M.; Ritala, M. Atomic Layer Deposition (ALD): From Precursors to Thin Film Structures. In *Thin Solid Films*; Elsevier, 2002; Vol. 409, pp 138–146. https://doi.org/10.1016/S0040-6090(02)00117-7.
- (33) Arduengo, A. J.; Harlow, R. L.; Kline, M. A Stable Crystalline Carbene. *J. Am. Chem. Soc.* **1991**, *113* (1), 361–363. https://doi.org/10.1021/ja00001a054.
- (34) Crudden, C. M.; Allen, D. P. Stability and Reactivity of N-Heterocyclic Carbene Complexes. *Coordination Chemistry Reviews*. December 2004, pp 2247–2273. https://doi.org/10.1016/j.ccr.2004.05.013.
- (35) Crudden, C. M.; Horton, J. H.; Ebralidze, I. I.; Zenkina, O. V; Mclean, A. B.; Drevniok, B.; She, Z.; Kraatz, H.-B.; Mosey, N. J.; Seki, T.; et al. Ultra Stable Self-Assembled Monolayers of N-Heterocyclic Carbenes on Gold. *Nat. Chem.* | **2014**, 6. https://doi.org/10.1038/NCHEM.1891.
- (36) Larrea, C. R.; Baddeley, C. J.; Narouz, M. R.; Mosey, N. J.; Horton, J. H.; Crudden,
 C. M. N -Heterocyclic Carbene Self-Assembled Monolayers on Copper and Gold:
 Dramatic Effect of Wingtip Groups on Binding, Orientation and Assembly.
 ChemPhysChem
 2017,
 18 (24),
 3536–3539.

- https://doi.org/10.1002/cphc.201701045.
- (37) Saba, S.; Brescia, A. M.; Kaloustian, M. K. One-Pot Synthesis of Cyclic Amidinium Tetrafluoroborates and Hexafluorophosphates; the Simplest Models of N5,N100methenyltetrahydrofolate Coenzyme. *Tetrahedron Lett.* **1991**, 32 (38), 5031–5034. https://doi.org/10.1016/S0040-4039(00)93420-8.
- (38) Dubinina, G. G.; Furutachi, H.; Vicic, D. A. Active Trifluoromethylating Agents from Well-Defined Copper(I)-CF 3 Complexes. *J. Am. Chem. Soc.* **2008**, *130* (27), 8600–8601. https://doi.org/10.1021/ja802946s.
- (39) Griffiths, M. B. E.; Dubrawski, Z. S.; Bačić, G.; Japahuge, A.; Masuda, J. D.; Zeng, T.; Barry, S. T. Controlling the Thermal Stability and Volatility of Organogold(I) Compounds for Vapor Deposition with Complementary Ligand Design. *Eur. J. Inorg. Chem.* 2019, 2019 (46), 4927–4938. https://doi.org/10.1002/ejic.201901087.
- (40) Dussarrat, C.; Wilmington. Bis-Ketoiminate Copper Precursors for Deposition of Copper-Containing Films and Methods Thereof. *United States Patient*. Patient Number: US 9,121,093 B2.
- (41) Rahtu, A.; Alaranta, T.; Ritala, M. In Situ Quartz Crystal Microbalance and Quadrupole Mass Spectrometry Studies of Atomic Layer Deposition of Aluminum Oxide from Trimethylaluminum and Water. 2001. https://doi.org/10.1021/la010103a.

6 APPENDICIES

Appendix A

Key labeled spectroscopic data for compounds **1-5** are shown below.

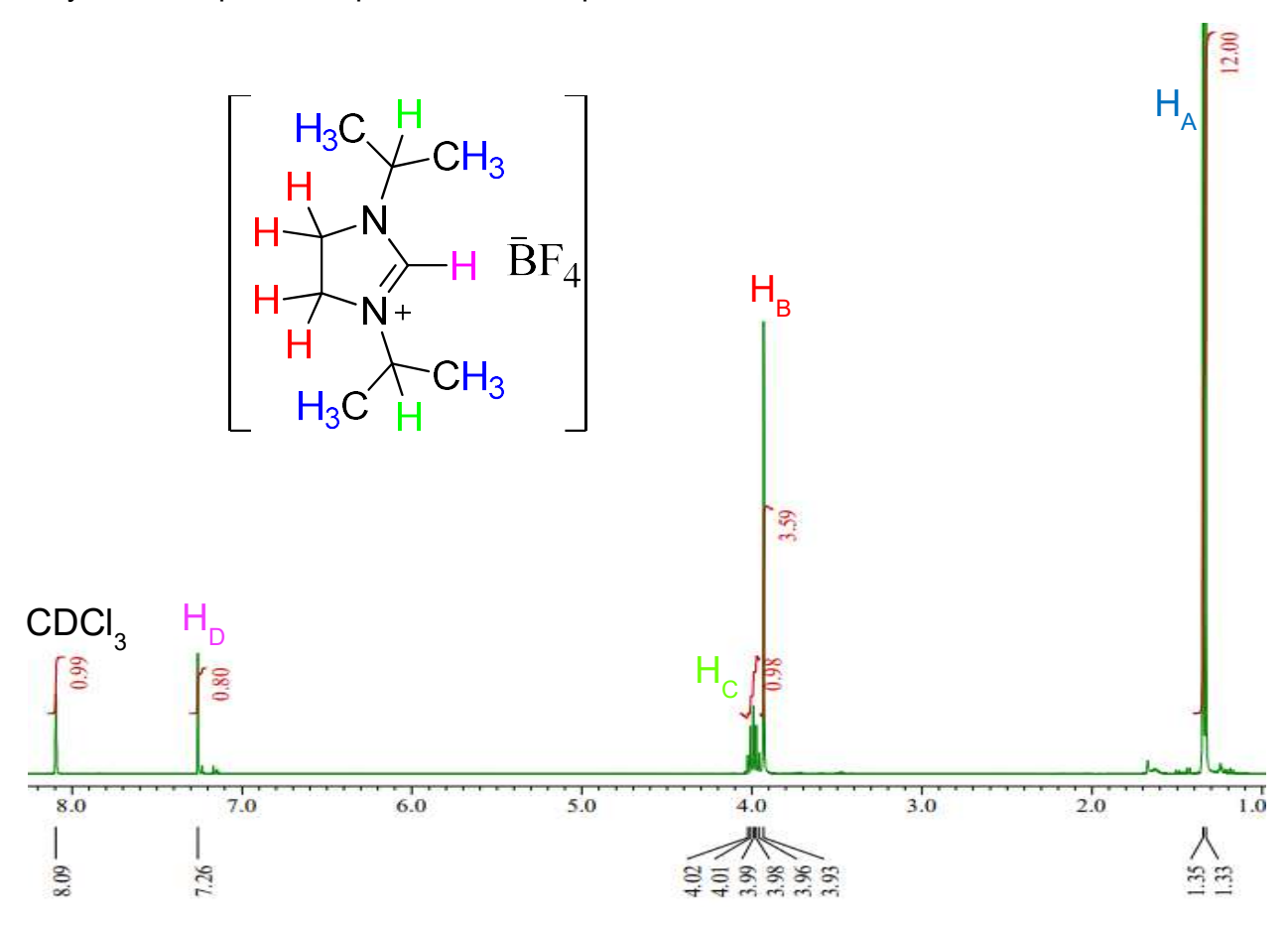


Figure 15. ¹H NMR of compound 1 in CDCl₃

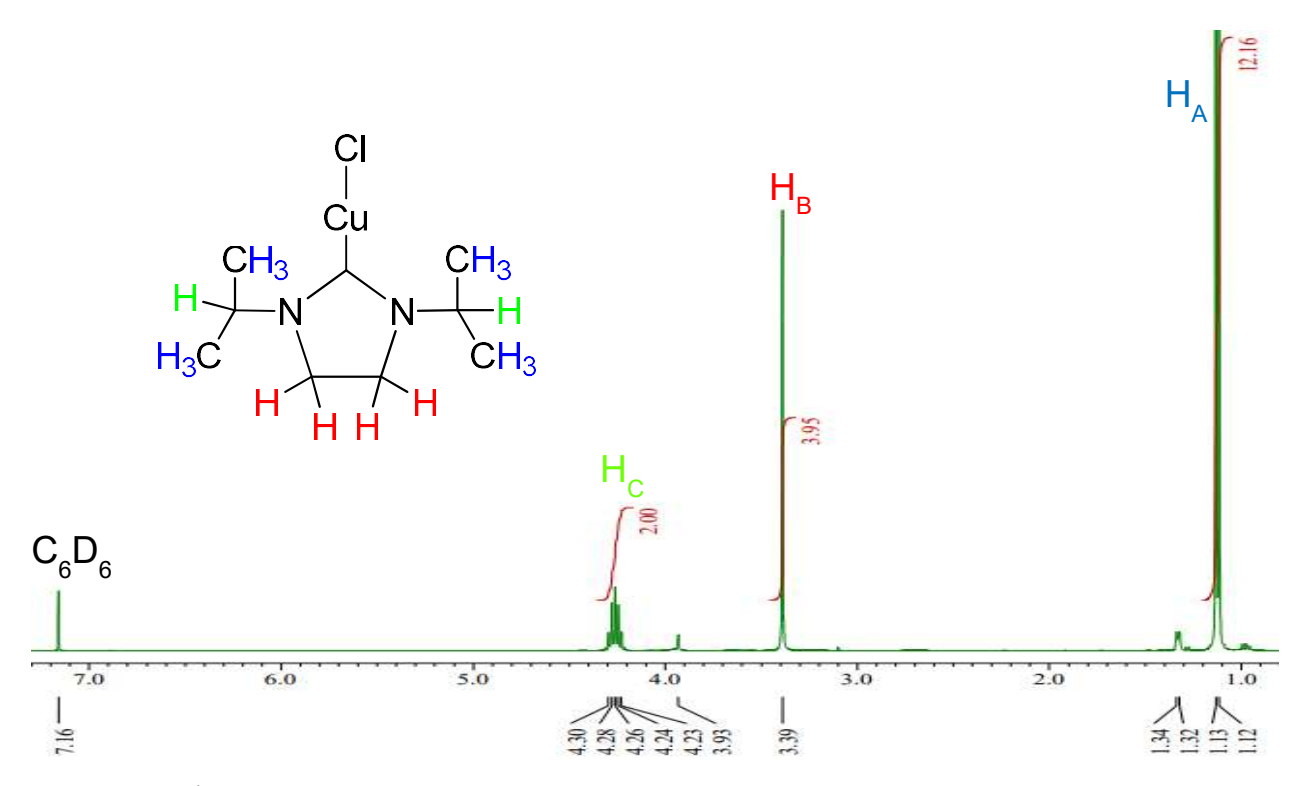


Figure 16. ¹H NMR of compound 2 in C₆D₆

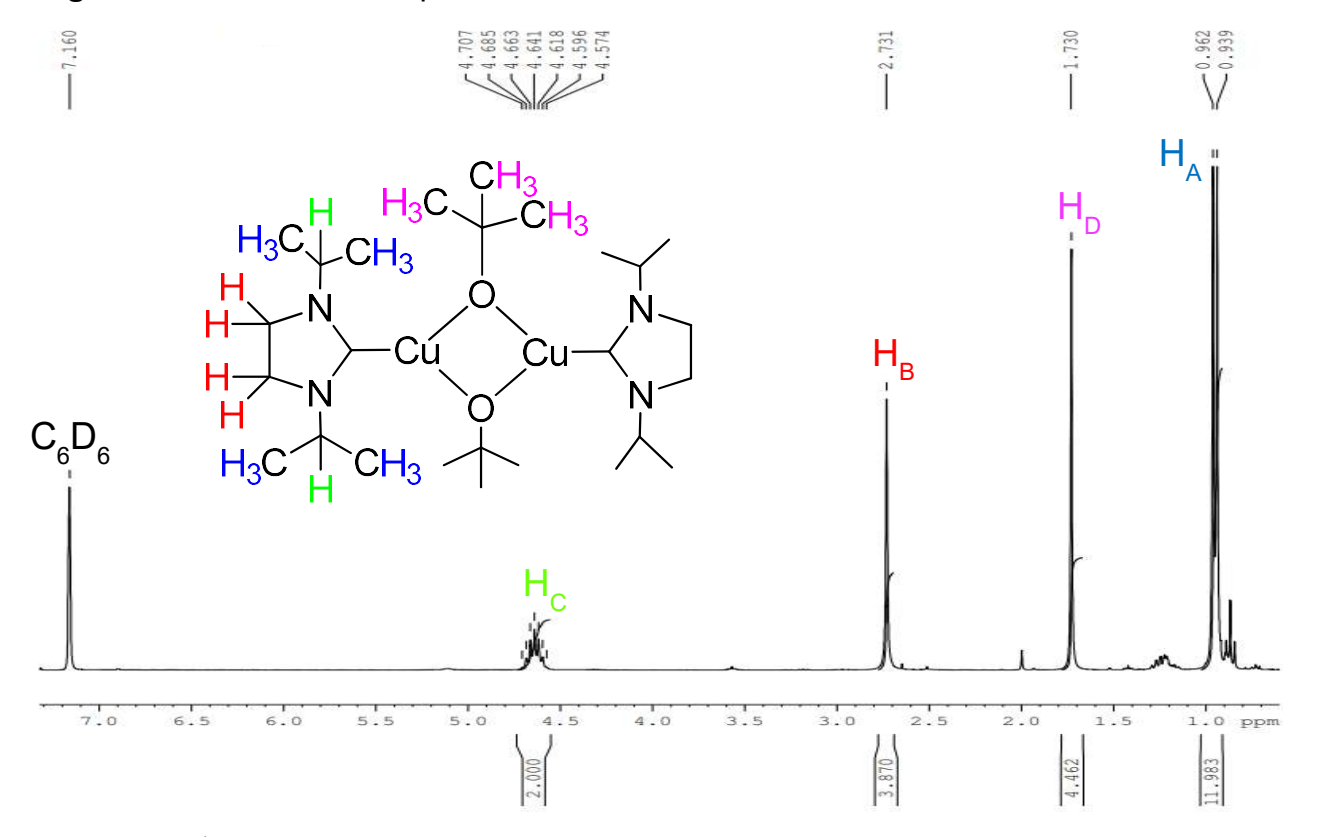


Figure 17. 1H NMR of compound 3 in C_6D_6

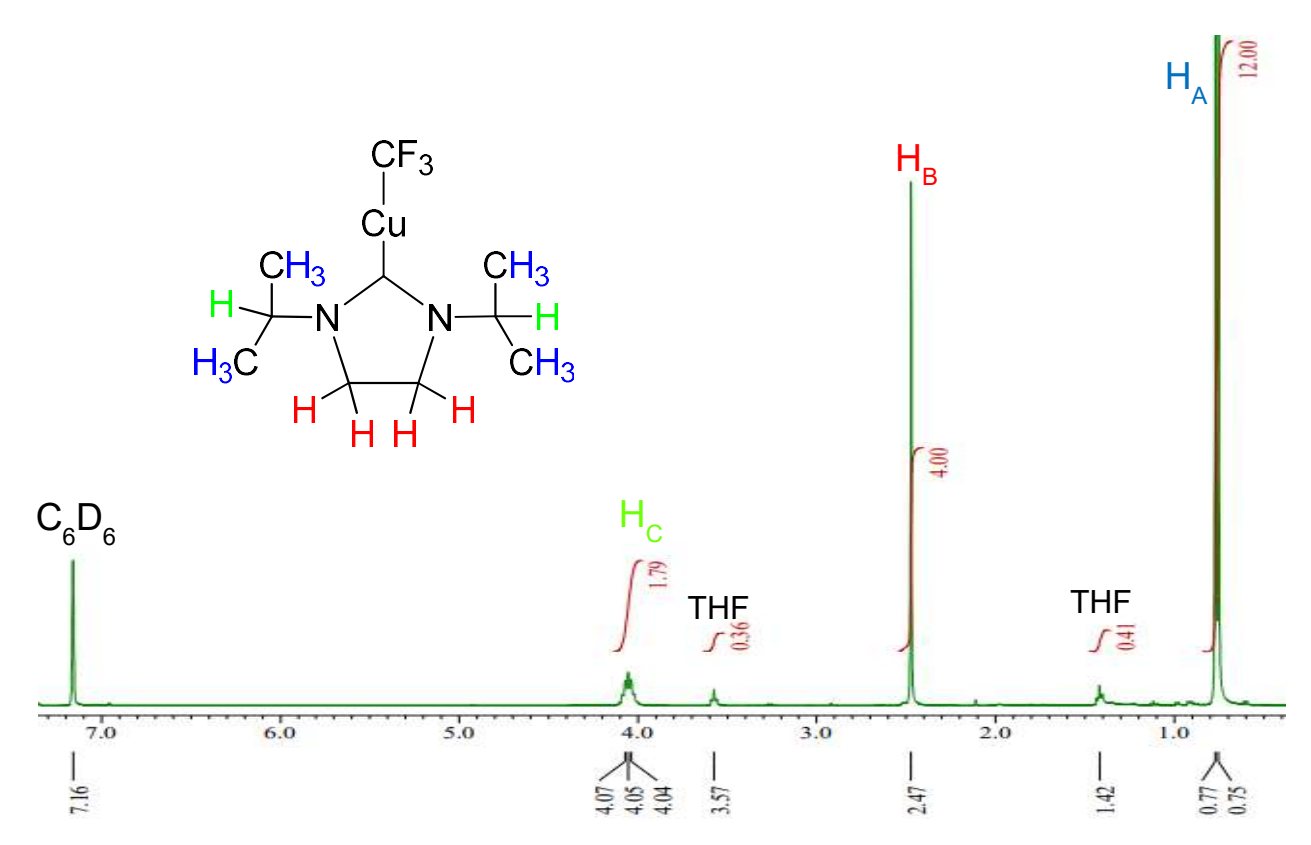


Figure 18. ¹H NMR of compound 4 in C₆D₆

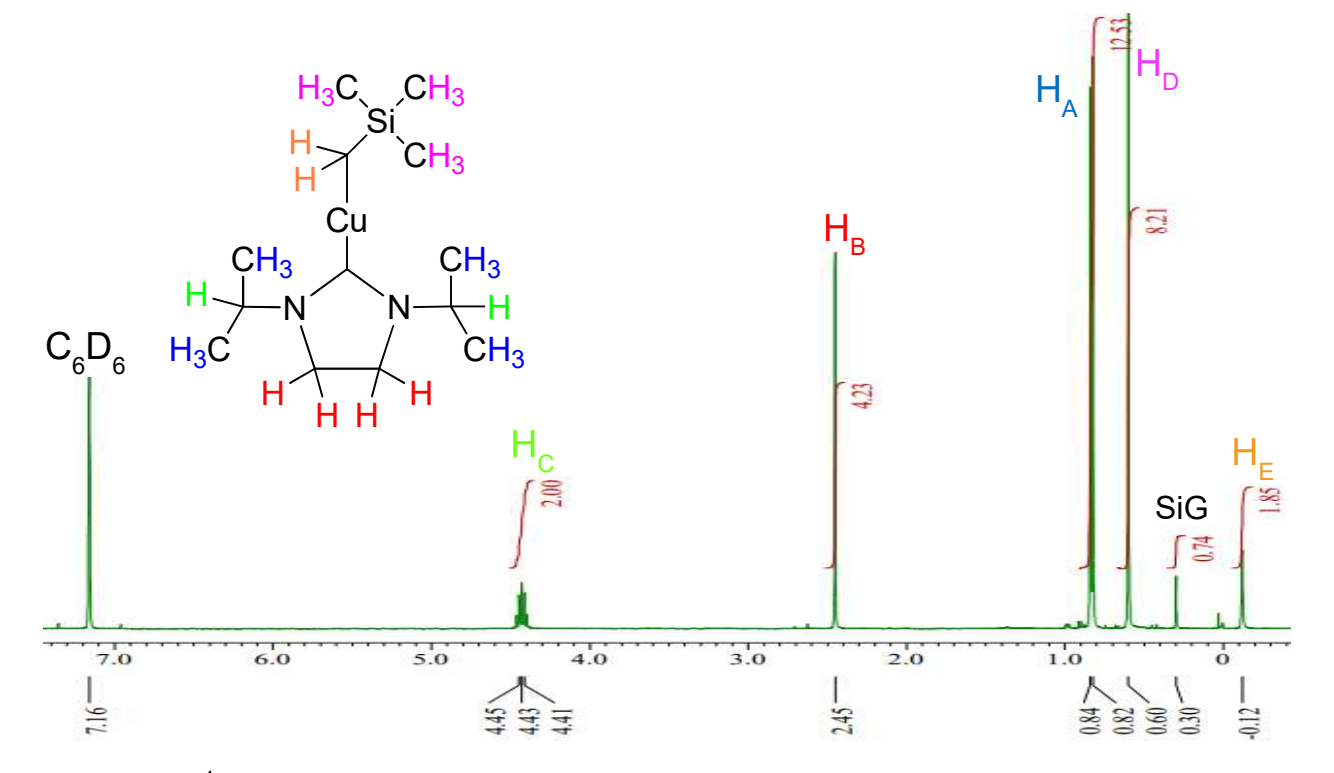


Figure 19. ¹H NMR of compound 5 in C₆D₆

Appendix B

All crystal structures in this work were produced by Prof. Jason D. Masuda.

Prof. Jason Masuda
Department of Chemistry
Saint Mary's University
923 Robie St.
Halifax, NS
B3H 3C3

General Method

A crystal of the compound in question was mounted from Paratone-N oil on an appropriately sized MiTeGen MicroMount. The data was collected on a Bruker APEX II charge-coupled-device (CCD) diffractometer, with an Oxford 700 Cryocool sample cooling device. The instrument was equipped with graphitemonochromated Mo K α radiation (λ = 0.71073 Å; 30 mA, 50 mV), with MonoCap X-ray source optics. For data collection, four ω -scan frame series were collected with 0.5° wide scans, 5-30 second frames and 366 frames per series at varying ϕ angles (ϕ = 0°, 90°, 180°, 270°). Data collection, unit cell refinement, data processing and multi-scan absorption correction were applied using the APEX2¹ or APEX3² software packages. The structures were solved using SHELXT³ and all non-hydrogen atoms were refined anisotropically with SHELXL⁴ using a combination of shelXle⁵ and OLEX2⁶ graphical user interfaces. Unless otherwise noted, all hydrogen atom positions were idealized and ride on the atom to which they

were attached. The final refinement included anisotropic temperature factors on all nonhydrogen atoms.

Crystallographic References

- Bruker, APEX2, SAINT, and SADABS. Bruker AXS Inc. Madison Wisconsin, USA., 2008.
- 2. Bruker, APEX3, SAINT, and SADABS Bruker AXS Inc., Madison, Wisconsin, USA, 2016.
- G. M. Sheldrick, Acta Crystallographica Section A, 2015, 71, 3-8
 (DOI:10.1107/S2053273314026370).
- G. M. Sheldrick, Acta Crystallographica Section C, 2015, 71, 3-8
 (DOI:10.1107/S2053229614024218).
- 5. C. B. H\ubschle, G. M. Sheldrick and B. Dittrich, *Journal of Applied Crystallography*, 2011, **44**, 1281-1284 (DOI:10.1107/S0021889811043202).
- O. V. Dolomanov, L. J. Bourhis, R. J. Gildea, J. A. K. Howard and H. Puschmann, *Journal of Applied Crystallography*, 2009, 42, 339-341
 (DOI:10.1107/S0021889808042726).